공학석사 학위논문

# Simple and Effective Gas-Phase Doping for Lithium Metal Protection in Lithium Metal Batteries

리튬 금속 배터리의 리튬 금속 보호를 위한 간단하고

효과적인 가스상 도핑

2018 년 2 월

서울대학교 대학원

재료공학부

문 세 환

# Simple and Effective Gas-Phase Doping for Lithium Metal Protection in Lithium Metal Batteries

리튬 금속 배터리의 리튬 금속 보호를 위한 간단하고 효과적인 가스상 도핑

지도교수 강 기 석

이 논문을 공학석사 학위논문으로 제출함

2018 년 2 월

서울대학교 대학원

재료공학부

문 세 환

문 세 환의 석사 학위논문을 인준함

**2018** 년 2 월

위 원 장 박 병 우 (인)

부위원장 강 기 석 (인)

위 원 최 장 욱 (인)

## Abstract

# Simple and Effective Gas-Phase Doping for Lithium Metal Protection in Lithium Metal Batteries

Moon, Sehwan

Department of Material Science and Engineering

College of Engineering

The Graduate School

Seoul National University

Increasing demands for advanced lithium batteries with higher energy density have resurrected the use of lithium metal as an anode, whose practical implementation has still been restricted, because of its intrinsic problems originating from the high reactivity of elemental lithium metal. Herein, we explore a facile strategy of doping gas phase into electrolyte to stabilize lithium metal and suppress the selective lithium growth through the formation of stable and homogeneous solid electrolyte interphase (SEI) layer. We find that the sulfur dioxide gas additive doped in electrolyte significantly improves both chemical and electrochemical stability of lithium metal electrodes. It is demonstrated that the cycle stability of the lithium cells can be remarkably prolonged, because of the compact and homogeneous SEI layers consisting of Li−S−O reduction products formed on the lithium metal surface. Simulations

on the lithium metal growth process suggested the homogeneity of the protective layer induced by the gas-phase doping is attributable for the effective prevention of the selective growth of lithium metal. This study introduces a new simple approach to stabilize the lithium metal electrode with gas-phase doping, where the SEI layer can be rationally tunable by the composition of gas phase.

**Keywords : lithium rechargeable battery, sulfur dioxide, gas additive, gas phase doping, solid electrolyte interphase layer, chemical/electrochemical stability, uniform $Li^+$ diffusion**

**Student Number : 2016-20850**

# Contents

# List of Tables

# List of Figures

**Figure 6.** Galvanostatic cycling performance of Li/Li symmetric cells (a) at 0.056 mA $cm^{-2}$ and (b) at 0.5 mA $cm^{-2}$ in 1 M $LiPF_6$/TEGDME. Blue and red indicates bare cells and sulfur dioxide-doped cells, respectively. (c) Impedance spectra of Li/Li symmetric cells with (red) and without (blue) sulfur dioxide doping before cycling. (d) The overall resistance changes of Li/Li symmetric cell, as a function of the cycle number for each electrolyte system.

**Figure 7.** Galvanostatic cycling performance of Li/Li symmetric cells at 1.0 mA $cm^{-2}$ in 1M $LiPF_6$/EC: DMC (volume by 1:1).

**Figure 8.** Electrolyte properties change in different electrolytes when sulfur dioxide bubbled. (a) Solvent dielectric constant (b) electrolyte viscosity (c) electrolyte ionic conductivity were measured at 20 °C.

**Figure 9.** Impedance spectra comparison of Li/Li symmetric cell with and without sulfur dioxide additive in electrolytes (a) before cycle (b) after 10 cycles (c) after 30 cycles (d) after 60 cycles (e) after 100 cycles (f) after 132 cycles (g) after 165 cycles (h) after 206 cycles.

**Figure 10.** SEM images of the surface morphologies of lithium metals (a) before cycle, (b) after 9 cycles, and (c) after 69 cycles in bare cells, as well as (d) before cycle, (e) after 9 cycles, and (f) 69 cycles in sulfur-dioxide-doped cells at a current density of 2 mA $cm^{-2}$. (g) Elemental EDS mapping images of SEI film isolated on stainless steel substrate. Color mapping of yellow, blue, pink, green, and red denote sulfur, carbon, oxygen, fluorine, and phosphorus elements, respectively. The S2p XPS spectra of the Li electrode (h) before sputtering and (i) after 300 s of sputtering. These XPS specimens,

obtained from Li/Li symmetric cells, experienced 9 cycles in sulfur-dioxide-containing electrolytes at 1 mA $cm^{-2}$.

**Figure 11**. (a) XPS Depth profile of S2p peak for the lithium surface. (left – bare cell, right – sulfur dioxide doped cell) (b) XPS Depth profile of C1s peak for the lithium surface. (left – bare cell, right – sulfur dioxide doped cell) (c) XPS Depth profile of F1s peak for the lithium surface (left – bare cell, right – sulfur dioxide doped cell) (d) XPS Depth profile of Li1s peak for the lithium surface. (left – bare cell, right – sulfur dioxide doped cell) (e) XPS Depth profile of O1s peak for the lithium surface. (left – bare cell, right – sulfur dioxide doped cell)

**Figure 12.** (a) Short-circuit time ($T_{sc}$) from galvanostatic measurement for Li/Li symmetric cells with a donut-shaped ring at various current densities ((■) bare cell and (□) sulfur dioxide-doped cell). The cell configuration for the sandwich cell is shown in the inset. Schematic mechanism of repeated deposition/dissolution processes in (b) bare cell and (c) sulfur dioxide-doped cell. Numerical simulation results of Li deposition under (d) irregular SEI and (e) regular SEI layers. Background color indicates the concentration of Li ions. White line is equipotential line in the electrolyte, and the red arrow describes the direction and the size of the current density.

**Figure 13.** Typical time dependent voltage profile of sandwich cells with (a) Bare cells and (b) sulfur dioxide doped cells at different current densities. Dot lines indicate the first voltage fluctuation by internal short circuit. (c) Calculation of vertical lithium growth rate based on Tsc values at different current density. (Filled – bare cell, Blank – sulfur dioxide doped cell)

**Figure 14.** (a) Voltage profiles of lithium metal full cells ($LiCoO_2$/300 μm of lithium) for the initial 2−5 cycles. Magnified voltage profiles of (b) charge part and (c) discharge part of panel (a). (d) Retention capacity and Coulombic efficiencies of a $LiCoO_2$/20 μm lithium cell with and without sulfur dioxide doping at 1C-rate (NP ratio 5).

**Figure 15.** Capacity degradation curves of (a) $LiCoO_2$ / lithium metal (300 μm) cell (b) $LiFePO_4$ / lithium metal (300 μm) cell with a 1 M $LiPF_6$ in EC/DMC (1:1 by volume).

**Figure 16.** Element mapping of lithium surface via Energy-dispersive X-ray spectroscopy (EDS). Each lithium metals were obtained from (a) after 400 cycles of $LiCoO_2$ / Excess lithium metal (b) after 350 cycles of $LiFePO_4$ / Excess lithium metal with a 1 M $LiPF_6$ in EC: DMC (1:1 by volume) with sulfur dioxide modified electrolyte.

**Figure 17.** Voltage profiles of $LiCoO_2$ / Lithium cell corresponding each cycle numbers (a) without (b) with sulfur dioxide additives under NP ratio 5.

**Figure 18.** Voltage profile of Li-symmetric cell with different electrolyte as a function of operation time. This graph shows the synergetic effect of supersaturated and sulfur dioxide doping.

# Chapter 1. Introduction

(The content of this chapter has been published in *Chemistry of Materials*. Reproduced with permission from [Moon, S *et al.*, *Chemistry of Materials,* **2017**, 29 (21), 9182–9191)

## 1.1 Introduction and outline

Elemental lithium metal has received much attention as an ideal high-energy-density negative electrode material for lithium batteries, because of the highest theoretical specific capacity (3860 mAh $g^{-1}$) and the lowest negative electrochemical potential (−3.040 V vs standard hydrogen electrode).[1−3] While these latent merits have been significantly plagued by the catastrophic safety issues of lithium metal anodes, which are tied to chronic problems such as (1) lithium dendritic growth and (2) the high reactivity of metallic lithium in electrolyte, recent intense demands for rechargeable batteries with higher energy density have made lithium metal come into the spotlight again. Moreover, various next-generation batteries, including lithium−sulfur (Li−S) and lithium−oxygen ($Li-O_2$) systems with exceptionally high energy density heavily rely on the stable cycling of lithium metal electrode.[4−7] Thus, the utilization of lithium metal anode in rechargeable system is pivotal not only for the further development of lithium "ion" batteries employing high-energy lithium metal anodes, but also for the realization of the next-generation battery chemistries.

Various chemical[8−21] as well as physical approaches[22−28] have been proposed to overcome the obstacles of metallic lithium metal anode. Attempts were made to introduce a physical barrier to protect the lithium metal surface via the deposition of film to inhibit protruding lithium growth. For instance, Zheng *et al.* employed the hollow carbon nanospheres with high shear modulus to block the dendrite penetration,[26] and Kazyak *et al.* investigated inorganic film coating such as $Al_2O_3$ thin layer via the atomic layer deposition method.[29] Organic additives, which are commonly used to stabilize the SEI layers of graphite anode in present lithium-ion batteries, have also been investigated to suppress undesirable electrolyte decomposition on the lithium metal electrodes,[8−10] such as vinylene carbonate (VC),[30,31] fluoroethylene carbonate (FEC),[32,33] and

succinic anhydrides (SA).[34,35] These additives were designed to decompose to a thin organic layer to protect the lithium metal surface during the electrochemical cycles. While these approaches could protect the lithium metal surface, thereby enhancing the cycle stability to some extent, the organic layer induced by additives was insufficient to protect the lithium metal anode involving a continuous volume change with newly exposed surface in repeated deposition/stripping processes, also the physical protective layer should be fabricated in the controlled atmosphere and the multilevel manufacturing processes generally brought out a major cause of increasing unit cell cost. Furthermore, physical film components inevitably accompany the reduction of overall energy density, because of additional weight and volume. Alternatively, Yamada *et al.* and Qian *et al.* recently demonstrated that the undesirable lithium growth could be suppressed by simply increasing salt concentration in nonaqueous electrolyte, which enhances the stability of the electrolyte itself against the lithium metal.[21,36] Nevertheless, other issues, such as low ionic conductivity and high viscosity of the electrolyte, along with the use of a large amount of high-cost salts, remain as hurdles for the employment of super-concentrated electrolyte.

Herein, we propose a facile and cost-effective approach to stabilize lithium metal anode using gas-phase doping to the electrolyte. We find that the use of gaseous sulfur dioxide as an electrolyte additive is particularly effective for enhancing the chemical/electrochemical stability of the lithium metal surface among various gas additives. The surface analyses reveal that the reduction of sulfur dioxide gas occurs on the lithium metal and produces a thin layer of inorganic Li−S−O compounds, which aids in the development of artificially uniform SEI layers. It also leads to a homogeneous supply of Li ions to the lithium electrode throughout the uniform SEI layer. Furthermore, the applicability of sulfur-dioxide-induced protection layer is examined in several electrolyte systems, including acetonitrile based electrolytes, which are highly reactive with lithium metal, confirming the simple and effective gas doping strategy to stabilize lithium metal electrode for various types of lithium batteries. This finding of the enhancement of lithium metal stability using sulfur dioxide gas also suggests the underlying reason for the remarkably long calendar life and high efficiency of lithium−sulfur dioxide primary batteries that have been developed in the 1970s.[37,38] Revisiting this demonstrates that stable and homogeneous protection

layers on the lithium metal induced by sulfur dioxide additives efficiently suppress the selective growth of lithium and provides a detailed mechanistic study, using the combined experimental and computational investigations.

# Chapter 2. Experimental

## 2.1 Preparation of gas-phase doping electrolyte

Lithium bis(trifluoromethane)- sulfonamide (LiTFSI), tetraethylene glycol dimethyl ether (TEGDME), and acetonitrile were purchased from Sigma−Aldrich. Commercial 1M $LiPF_6$ in ethylene carbonate/dimethyl carbonate (volume ratio = 1:1) mixture and sulfur dioxide gas (purity >99%) was used to prepare sulfur-dioxide-bubbled electrolyte. The moisture content of electrolyte was controlled under 20 ppm, which was measured by using Karl Fischer titration. To fix the quantity of sulfur dioxide in the electrolyte, bubbling time was strictly controlled for 5 min with a pressure of 0.5 bar. A schematic diagram of the bubbling process, as well as the detailed setting for the bubbling of sulfur dioxide, are shown in Table 1 and Figure 1.

| Solubility of $SO_2$, mg/ml | 1min bubbling | 5min bubbling | 15min bubbling | 30min bubbling | 60min bubbling |
|---|---|---|---|---|---|
| 1M $LiPF_6$ in EC/DMC | 18.7 | 38.6 | 66.2 | 94.8 | 112.7 |
| 1M $LiPF_6$ in TEGDME | 73.1 | 141.4 | 184.0 | 223.1 | 281.8 |
| 1M LiTFSI in Acetonitrile | 95.7 | 128.1 | 151.0 | 183.5 | 220.6 |

※ Sulfur dioxide bubbling under 0.5 bar pressure

**Table 1.** Sulfur dioxide solubility measurement in different electrolyte systems.

(a)

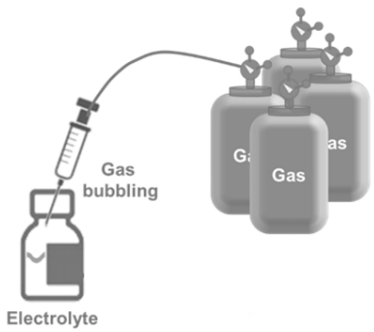


(b)

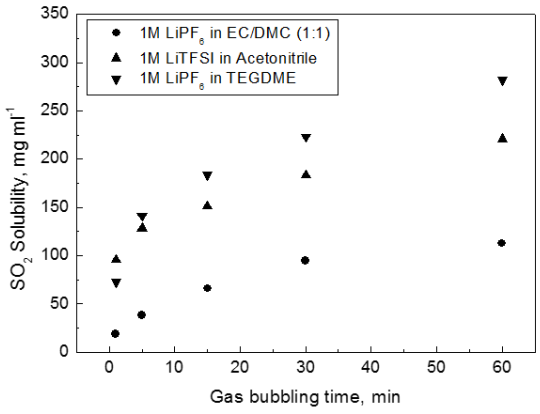

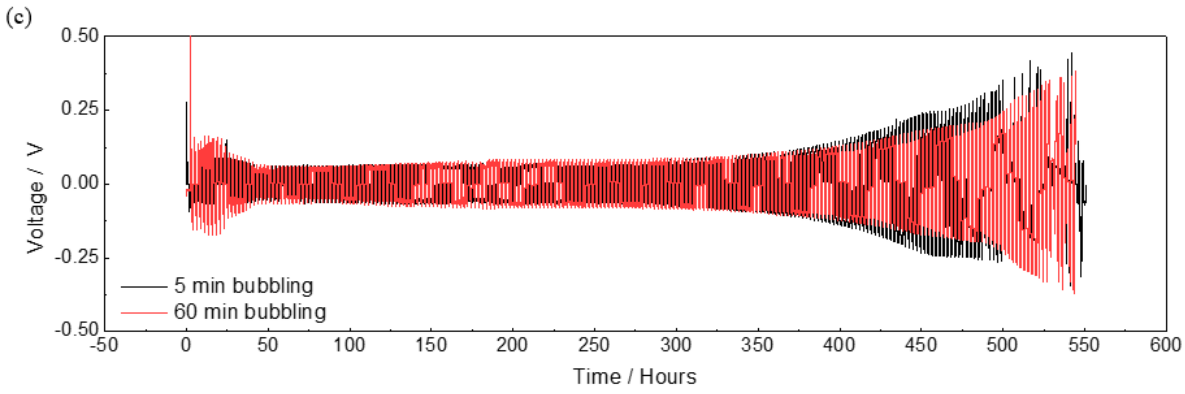


**Figure 1.** (a) Schematic diagram of gas injection method into electrolyte. (b) Sulfur dioxide solubility measurement in different electrolyte systems. (c) Galvanostatic cycling performance of Li/Li symmetric cells with current density 0.5 mA $cm^{-2}$ after 5 and 60 minutes sulfur dioxide bubbling.

**Discussion on Figure 1.** Based on cycle performance in $LiPF_6$ EC/DMC, sulfur dioxide doping time was carefully set to 5 minutes with 0.5 bar. Even though the electrolyte bubbled with sulfur dioxide for 60 minutes contains much higher content of sulfur dioxide, there is no significant difference in cycle life of lithium symmetric cells depending on the concentration of sulfur dioxide. By a simple measurement of the mass change of EC/DMC electrolyte after sulfur dioxide addition, the electrolytes bubbled for 5 and 60 minutes contain 0.6025 M and 1.759 M of sulfur dioxide, respectively. These values can be regarded as a significantly high concentration, compared to that of poly sulfide additives whose maximum concentration was 0.18 M due to the solubility limits in a previous report.[55] Therefore, we believe that relatively short gas bubbling time of 5 minute is sufficient to provide such a high sulfur dioxide content to protect lithium metal surface.

## 2.2 Fabrication of coin cell

For Li/Li symmetric test, electrochemical cells were assembled in an Ar-filled glovebox using a CR2032-type coin cell with 300-μm-thick Li foil as the counter and working electrodes. Customized PVDF rings (outer diameter = 16.5 mm, inner diameter = 8 mm, thickness = 100 μm) were prepared to build sandwich cells. To evaluate a full cell system, $LiCoO_2$ ($LiCoO_2$, Super-P, PVDF weight ratio = 92:4:4) and $LiFePO_4$ cathode active materials ($LiFePO_4$, Super-P, PVDF weight ratio = 7:2:1) were prepared by casting a paste on Al foil. The coated slurry on Al current collector was dried at 120 °C for 12 h and roll-pressed. Then, 2032 coin cells, which were composed of a $LiCoO_2$ or $LiFePO_4$ cathode, a glass fiber membrane (Whatman GF/F microfiber filter paper, USA) and the Li anode, were fabricated. Particularly, for a $LiCoO_2$, which operates at >4.0 V, artificial sulfur dioxide protection film was formed by using Li/Li symmetric cells through precycling in sulfur dioxide-doped electrolyte to avoid the oxidation of residual sulfur dioxide molecules in the electrolyte, details of which are discussed in Figure 2. The protected lithium obtained from the disassembled Li/Li symmetric cells were employed for the high voltage batteries with fresh electrolyte, which does not contain sulfur dioxide.

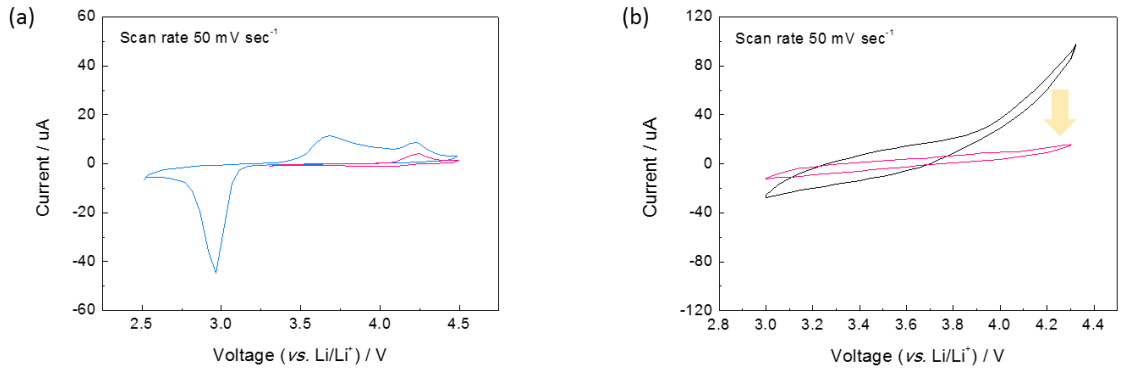


**Figure 2.** Three electrode cyclic voltammogram of sulfur dioxide - injected electrolyte from 2.5 V to 4.5 V (blue line) and from 3.3 V to 4.5 V (red line) at 50 mV $sec^{-1}$ scan rate. (b) Li/Al two electrodes cyclic voltammogram. Black line was measured when residual sulfur dioxide molecules are in electrolyte. Red line was measured when no residual sulfur dioxide molecules are in electrolyte. To eliminate all residual sulfur dioxide

molecules, coin cell was reassembled with fresh electrolyte after 9 cycles at 1mA $cm^{-2}$ in sulfur dioxide containing electrolyte.

**Discussion on the Figure 2.** In the presence of sulfur dioxide additive, a detectable cathodic peak evolves at 2.95 V, which is presumably a signal of reduction process of sulfur dioxide molecules, in consistent to discharge voltage of lithium-sulfur dioxide batteries. On the contrary, two small oxidation peaks are observed at 3.67 V and 4.24 V. First oxidation peak at 3.67 V would be assigned to the oxidation of sulfur dioxide relevant products which are formed during first reduction sweep. The second oxidizing current appeared at 4.24 V is regarded as oxidation process of residual sulfur dioxide molecules itself in the electrolyte considering that the reduction peak at 3.67 V disappears but the peak at 4.24 V still remains after altering voltages scanning range to 3.3 V~4.5 V (*vs.* $Li/Li^+$). This fact is also confirmed by two electrode system which is similar to the actual battery environment. This observation points out that sulfur dioxide additive should be used carefully under 4.0V without appropriate counter-measures. If the residual sulfur dioxide molecules in the electrolyte are thoroughly removed, a current indicating troublesome reaction over 4.0 V become invisible.

## 2.3 Characterization

For the determination of electrolyte properties, a viscosity meter (SV-10 viscometer, A&D Company Ltd. Japan), a dielectric constant meter (liquid dielectric constant meter model 871, Nihon Rufuto, Japan), and portable ionic conductivity (using a waterproof portable conductivity meter, Model CON 610, Oakton, Singapore) were used at 20 °C. The visual inspection experiments in 1M LiTFSI/acetonitrile electrolyte with various additives were observed in Ar-filled gloveboxes ($H_2O$ < 0.5 ppm, $O_2$ < 0.5 ppm). For the electrochemical Li/Li symmetric tests, constant current mode was applied within voltage range from 3.0 V to −3.0 V at various current

densities. In order to check the electrochemical stability of sulfur dioxide in electrolyte system, the cyclic voltammetry tests were conducted. The cyclic voltammetry tests of two electrodes consisting of lithium metal and Al current collector were performed under identical cell configuration of CR2032. In three electrode system, gold as working electrode and platinum as counter electrode and $Ag/Ag^{+}$ as reference electrode were used and applied scan rate was 50 mV/s. The surface morphologies of the Li electrode were measured by scanning electron microscopy (SUPRA 55VP, Carl Zeiss, Germany). To investigate interfacial resistance properties on lithium metal, electrochemical impedance spectroscopy was introduced for Li/Li symmetric cell from 300 MHz to 0.05 Hz (Model VSP-300, Bio-Logic Science Instruments, France). The compositional changes of SEI layer on lithium surface with depth were analyzed by X-ray photoelectron spectroscopy (XPS) (Thermo VG Scientific, Sigma Probe, U.K.). The electrochemical performances of cells were investigated using a potentio-galvanostat (Model WBCS 3000, WonA Tech, Korea) at room temperature.

## 2.4 Numerical simulation details

Numerical simulations on Li deposition process were performed using COMSOL electrodeposition model with tertiary Nernst−Planck interface. The model structure consists of Li metal, an electrolyte, a Cu current collector, and an SEI layer, as shown in Figure 3. A 100-nm-thick SEI layer covers the surface of the flat Cu current collector, and the SEI layer is divided into two sections in order to model the irregular composition and ionic diffusivity of SEI layer. Diffusion coefficient of Li ion in electrolyte is set to $7.5 \times 10^{-11}$ m2 $s^{-1}$. For the simulation of the bare cell and sulfur dioxide-doped cell, diffusivities are set to $1 \times 10^{-11}$ and $2.5 \times 10^{-12}$ $m^2$ $s^{-1}$, and $7.5 \times 10^{-12}$ and $5 \times 10^{-12}$ $m^2$ $s^{-1}$, respectively. The initial concentration of Li ion in the electrolyte is set to 1 M and the overpotential for Li deposition is set to 0.2 V.

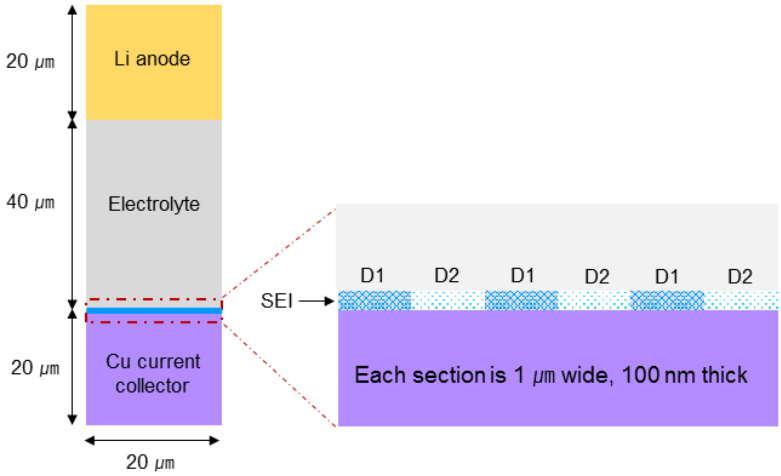


**Figure 3.** Schematic diagram of Numerical model system.

# Chapter 3. Results and discussion

## 3.1 Chemical/Electrochemical stability of lithium metal electrode protected by gas phase doping

A simple visual inspection test was set to examine the effect of additives on the chemical stability of lithium metals in the electrolytes. Acetonitrile-based electrolyte with LiTFSI salts was selected as a model electrolyte, because of its well-known vigorous reactivity with metallic lithium. The discoloration of acetonitrile electrolytes upon the side reaction makes it possible to visibly evaluate the chemical stability of lithium metal under different conditions, as shown in Figure 4. The evolution of bubbles was detected 5 min after soaking lithium metal in the bare acetonitrile electrolyte and the lithium metal completely disappeared after 30 min, as shown in Figure 4a, indicating the inherent instability. These corrosion reactions are expected to occur in a manner similar to that observed in other organic electrolytes, because of the thermodynamic instability of organic electrolytes toward the reductive metallic lithium, while the nature of intrinsic passivation layer would differ for each other and be critical for halting the corrosion.[39] The result in Figure 4a implies that the passivation layer on the lithium metal that formed upon exposure to acetonitrile could not halt the further corrosion, indicating that proper countermeasures are necessary in such electrolyte systems. In comparison, the same experiments were performed for electrolytes with previously reported additives, including 1 wt % LiNO3,[40−43] 5 wt % fluoroethylene carbonate (FEC)[7,10,15,44] and 30% LiF[45] in Figures 4b−d. These additives have been proven to be effective in protecting lithium metal electrode in conventional electrolyte. The chemical contact with lithium metal provides reductive conditions for the additives, which are thus expected to form a protective layer through decomposition on the electrode.1 Figures 4b−d show their intrinsic protective capability in the presence of lithium metal, which clearly indicates that, with the $LiNO_3$ and FEC additives, the stability of the lithium metal is noticeably enhanced. Unlike the bare electrolyte system, the lithium metal could be clearly visible without significant discoloration of the electrolyte after 60 min. However, after 1 day of storage, it was observed that the lithium metal was entirely dissolved in the electrolyte with the discoloration. In

the case of LiF additive, we could not witness a notable enhancement in the lithium metal stability, compared with the bare electrolyte in Figure 4d. In contrast, the chemical stability of the lithium metal was remarkably improved with the sulfur dioxide additive in Figure 4e. Even after a week of storage, there was no significant degradation of lithium metal or the discoloration of the electrolyte, implying that the protective layer that sulfur dioxide gas introduces can exhibit a superior stability over those induced by other additives even in such reactive acetonitrile (ACN)-based electrolytes.

The protective capability of sulfur dioxide additive was further examined under electrochemical cycling of Li/Li symmetric cell using 1 M LiTFSI/ACN electrolyte, as shown in Figure 4f. Without additives, a large polarization was observed as soon as the current is applied and a voltage reached the upper limit of 3.0 V (*vs.* $Li^+$/Li) within only a few cycles, which is attributed to the chemical instability of lithium metal as observed. Slight enhancement of the cycle stability was observed for the electrolyte systems, including $LiNO_3$ or FEC additives; however, the polarization was also enlarged within tens of cycles, which is consistent with the chemical stability tests that showed the dissolution of lithium metal within a few hours in the electrolyte. On the other hand, the cycle stability was notably improved with the sulfur dioxide gas additive with a relatively small polarization (~0.005 V), which was maintained over multiple stripping/deposition of lithium metal, as shown in Figures 4f and 4g. While the reversible electrochemical reaction of lithium metal in an acetonitrile has been believed to be impossible and was only recently demonstrated to be feasible using super-concentrated electrolyte by eliminating free solvent,[21] this observation indicates the efficacy of the lithium metal electrode protection using sulfur dioxide gas additive. It is also worth mentioning that the addition of sulfur dioxide does not significantly vary the ionic conductivity of the electrolyte, as shown in Figure 5, while the super-concentration substantially decreases the ionic conductivity of the electrolyte.[21] indicates that the intrinsic OER of superoxide phases would be more facile than those of peroxide phases assuming the absence of the charge transport limitation (electronic/ionic conductivity).

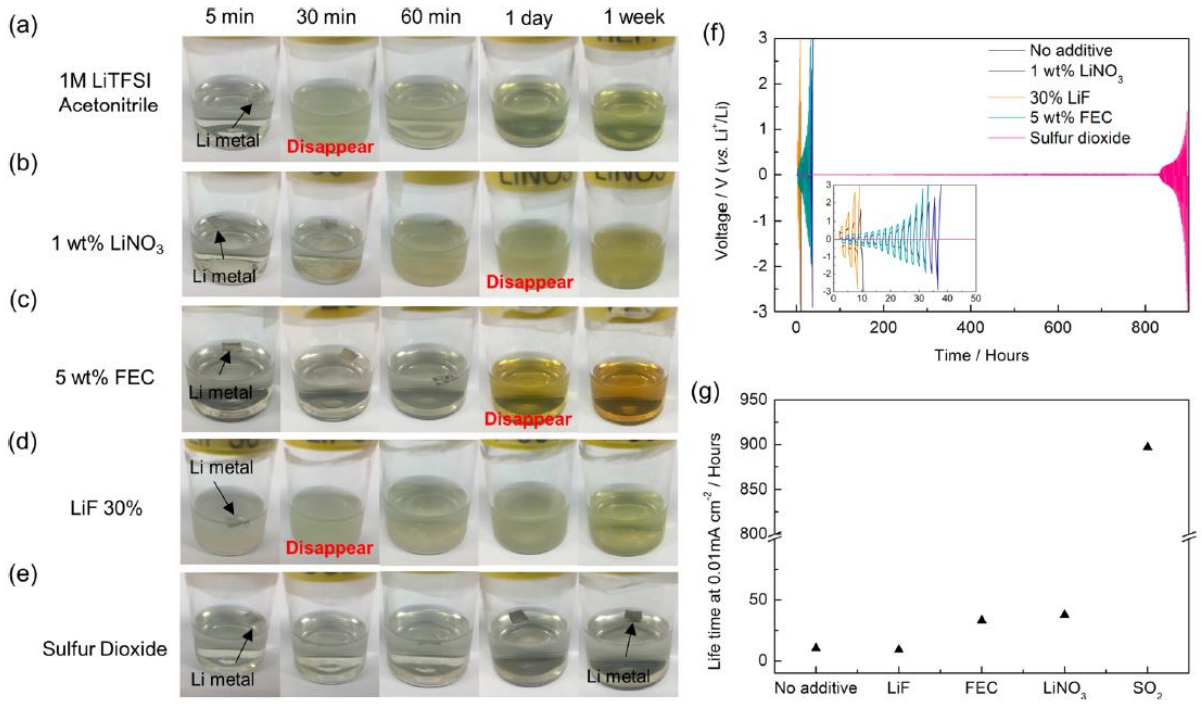


**Figure 4.** Photographs of lithium metal immersed in 1 M LiTFSI/acetonitrile at 25 °C over stored time (a) without any additive and with (b) 1 wt % $LiNO_3$, (c) 5 wt % FEC, (d) 30% LiF, and (e) sulfur dioxide. (f) Comparison of the voltage profiles of the Li/Li symmetric cell with different additives; the inset presents the zoomed-in short time region. (g) Cycle lifetimes of cells with various electrolytes (the cutoff voltage of 3.0 V or −3.0 V (*vs.* $Li^+$/Li)).

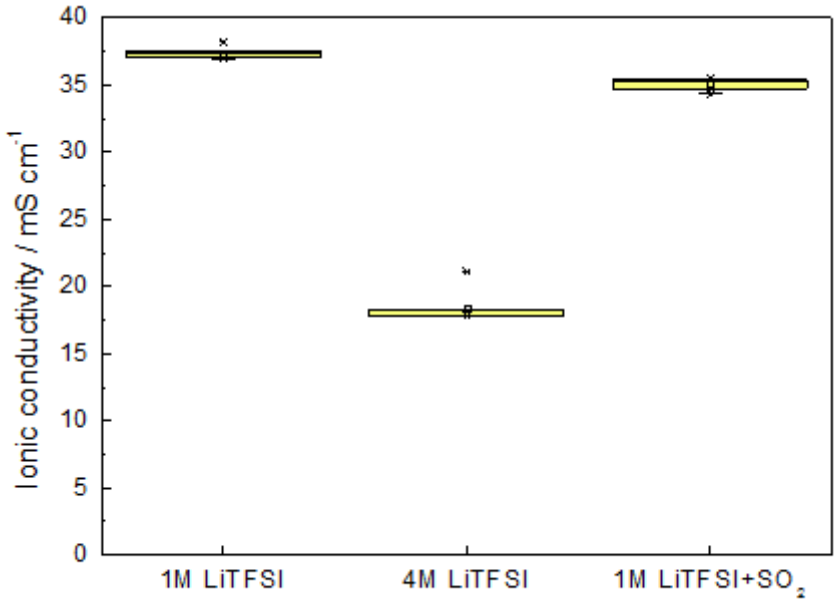


**Figure 5.** Ionic conductivity measurement of pure 1M and 4M LiTFSI in acetonitrile electrolyte

and sulfur dioxide bubbled 1M LiTFSI / Acetonitrile electrolyte.

The applicability of sulfur dioxide doping was additionally examined in other electrolyte systems. Figure 6a illustrates that the lithium metal electrode protection by gas-phase doping is also effective in ether-based electrolytes such as TEGDME, which are commonly used in lithium oxygen battery systems.[46,47] Without the sulfur dioxide doping, the polarization of a symmetric lithium cell gets larger with cycles and exhibits a dramatic increase at ~300 h; however, the lithium cell doped with sulfur dioxide maintains its low overpotential throughout the cycles in Figure 6a (~0.08 V polarization). At higher current rates (0.5 mA/cm$^2$), which involve more utilization of the lithium metal anode, the cycle stability of bare lithium cells gets noticeably degraded, showing the cycle termination within 30 h in Figure 6b, which is ascribed to a more roughened lithium metal surface and the correspondingly larger interface with the bare TEGDME electrolyte. On the other hand, the cycle stability significantly enhances up to more than 200 h with the sulfur dioxide doping maintaining ~0.2 V polarization. The feasibility was also examined in conventional carbonate-based electrolytes, as shown in Figure 7. It indicates that the doping of sulfur dioxide is also capable of protecting lithium metal electrode in conventional carbonate-based electrolytes, even at a higher current density of 1 mA cm$^{-2}$. Nevertheless, the improvement was not as dramatic as in the previous electrolyte systems, because of the relatively high stability of carbonate-based electrolytes against lithium metal.

The electrochemical impedance spectroscopy (EIS) in Figure 6c indicates that the enhanced stability and smaller polarization with sulfur dioxide additive is attributable to the reduction in the surface resistivity of lithium metals. Figure 6c presents the EIS results of two Li/Li symmetric cells with and without sulfur dioxide doping before cycling. The equivalent circuit for the analysis is provided in the inset of Figure 6c, which is composed of a bulk resistance ($R_b$) and two parallel circuits representing impedances from the surface film ($R_f$, $C_f$) and charge-transfer reaction ($R_{ct}$, $C_{ct}$), respectively. Although the Rf for bare lithium cells before cycling exhibited a value of 610 Ω, as shown in Figure 6c, interestingly, the surface film resistance for the cells doped with sulfur

dioxide was 190 Ω, which is approximately one-third of the value measured for the bare cell. It suggests that the interfacial property of the lithium metal was distinctly modified by simply immersing the lithium in the sulfur-dioxide doped electrolyte, even without the electrochemical reaction. The low $R_f$ value illustrates that it has induced the formation of a relatively conductive surface film on the lithium metal. On the other hand, the changes in $R_b$ (bulk resistance) and $R_{ct}$ (charge transfer) were not noticeable with and without the sulfur dioxide doping. The effect of other factors such as the change in the ionic conductivity of the electrolyte with additives was minimal (<10%), as shown in Table 2 and Figure 8. We further performed the EIS experiments with repeated cycles to probe the nature of new surface films deposited on the lithium metal electrode (Figure 9). It is well-known that the repeated stripping and deposition of lithium brings out fresh lithium metal exposed to the electrolyte every cycle, thus inducing the formation of a thicker surface film.[48−50] In order to model this scenario, we adopted a multilayer model circuit considering the additional surface film formation after cycles, which contains an extra impedance term, $R_{add}$ and $C_{add}$, corresponding to the impedance arising from the newly formed additional surface film, to the original equivalent circuit (see inset of Figure 6d). Figure 6d shows the overall resistance values as a function of cycles for the two lithium cells, which clearly illustrates that the surface film formed in the presence of the sulfur dioxide is consistently more conductive than that formed in the bare electrolyte. The more conductive nature of the surface film would reduce the growth of the polarization with cycles and enhance the cycle stability.

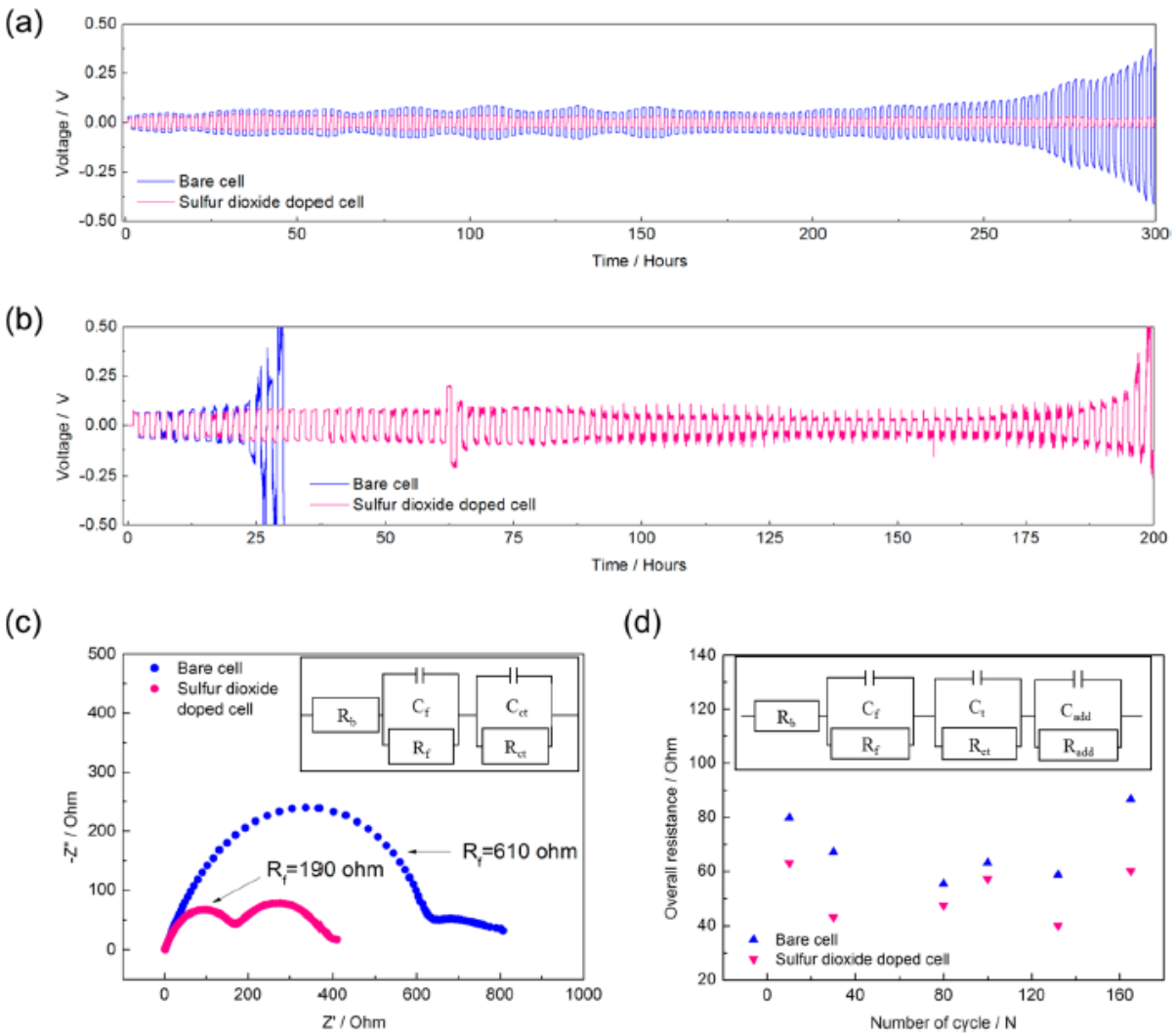


**Figure 6.** Galvanostatic cycling performance of Li/Li symmetric cells (a) at 0.056 mA $cm^{-2}$ and (b) at 0.5 mA $cm^{-2}$ in 1 M $LiPF_6$/TEGDME. Blue and red indicates bare cells and sulfur dioxide-doped cells, respectively. (c) Impedance spectra of Li/Li symmetric cells with (red) and without (blue) sulfur dioxide doping before cycling. (d) The overall resistance changes of Li/Li symmetric cell, as a function of the cycle number for each electrolyte system.

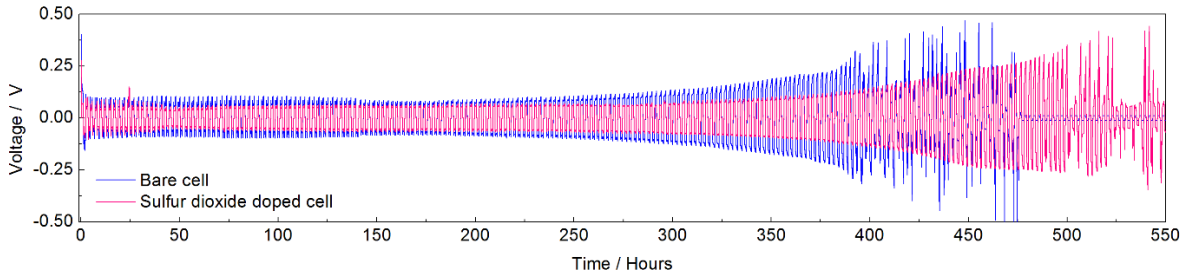


**Figure 7.** Galvanostatic cycling performance of Li/Li symmetric cells at 1.0 mA $cm^{-2}$ in 1M $LiPF_6$/EC: DMC (volume by 1:1).

| | 1M $LiPF_6$ in EC/DMC (v:v 1:1) | | 1M $LiPF_6$ in TEGDME | | 1M LiTFSI in Acetonitrile | |
|---|---|---|---|---|---|---|
| | Pure EL | $SO_2$ - EL | Pure EL | $SO_2$ - EL | Pure EL | $SO_2$ - EL |
| Viscosity, mPa*s | 4.11 | 3.59 | 7.69 | 8.19 | 1.09 | 1.37 |
| Dieletric constant (at 20°C) | 41.2 | 40.7 | 7.79 | 8.75 | 37.6 | 35.2 |
| Ionic conductivity, mS $cm^{-1}$ | 11.346 | 11.84 | 2.3236 | 2.6986 | 31.12 | 29.34 |

**Table 2.** Electrolyte properties change in different electrolytes when sulfur dioxide bubbled. All the values were measured at 20 °C.

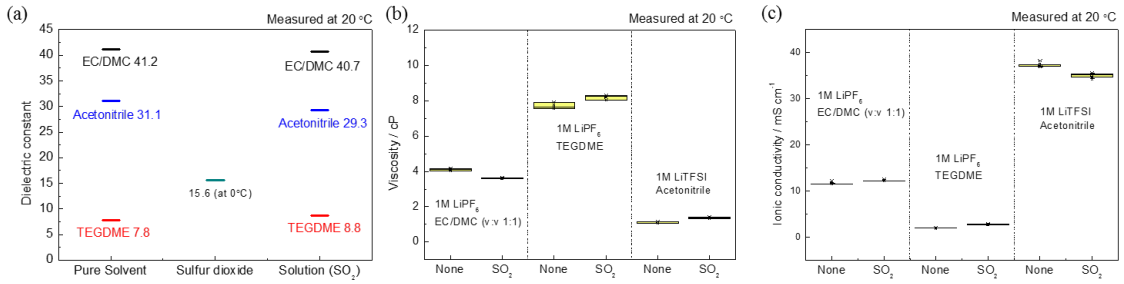


**Figure 8.** Electrolyte properties change in different electrolytes when sulfur dioxide bubbled. (a) Solvent dielectric constant (b) electrolyte viscosity (c) electrolyte ionic conductivity were measured at 20 °C.

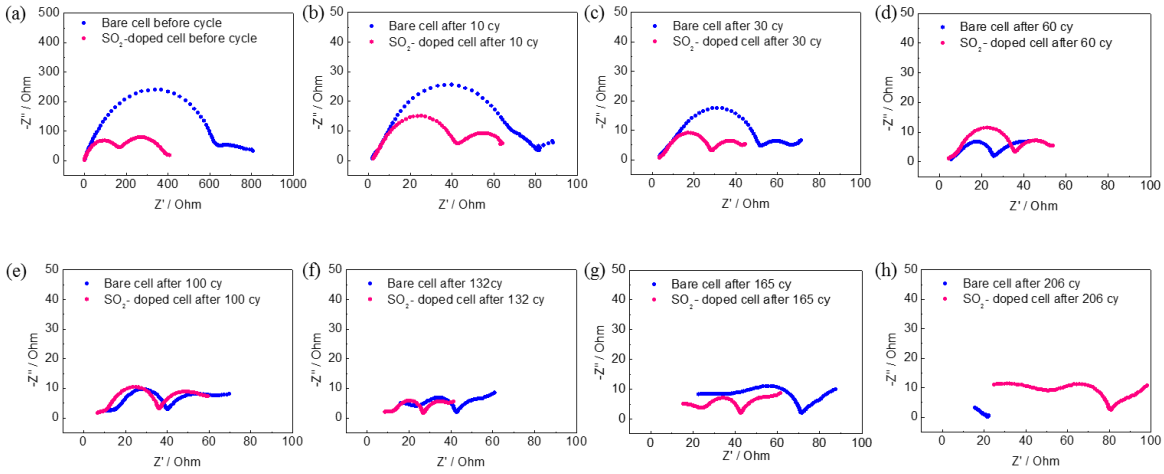


**Figure 9.** Impedance spectra comparison of Li/Li symmetric cell with and without sulfur dioxide additive in electrolytes (a) before cycle (b) after 10 cycles (c) after 30 cycles (d) after 60 cycles (e) after 100 cycles (f) after 132 cycles (g) after 165 cycles (h) after 206 cycles.

### 3.2 Nature of protection layer on the lithium

The surface morphologies were monitored via scanning electron microscopy (SEM) to understand the origin of the low surface resistance with sulfur dioxide doping. SEM images in Figure 10 depict the surfaces of lithium metal electrodes before cycle, after 9 cycles and 69 cycles of the bare cells (Figures 10a−c), along with those for the same cycles of the gas-doped cells (Figures 10d−f). Before the current is applied, there is no apparent difference in the surface morphology of both lithium metal electrodes, despite the observed difference in the surface film resistance before cycle in Figure 10c. The lithium metal surface in both cells gradually changes, with regard to the morphology, as the cycle proceeds. With the repeated electrochemical cycles, the surface of lithium metal using bare electrolyte became seriously porous and irregular, covered with selectively grown lithium (Figures 10b and 10c). These large surface areas generated by porous morphology provide reaction sites that can cause further side reactions and progressively thicken the surface film or SEI (solid electrolyte interphase) layer, leading to a growth of the cell impedance.[25,51−54] In contrast to the irregular lithium surface morphology, the lithium metal in the electrolyte doped with a sulfur dioxide additive displayed a much smoother surface after the repeated cycles, indicating the uniform lithium deposition/stripping reactions. This apparent distinction on the morphology is believed to be linked with the observed electrochemical behaviors in Figures 6c and 6d, where the electrode in the sulfur dioxide-doped electrolyte showed consistently lower surface resistance.

The characterization of SEI compositions and uniformity was further performed by using energy-dispersive X-ray spectroscopy (EDS). To investigate the initially formed SEI film without interference from lithium metals, we isolated the SEI film on a current collector substrate, following the lithium dissolution process of the first cycle, as previously suggested in the literature.[55] Elemental mapping image in Figure 10g shows that the SEI film in the presence of sulfur dioxide consists of elemental oxygen, carbon, fluorine, phosphorus, and sulfur, in contrast to the SEI of the bare cell, where no elemental sulfur exists. The significant amount of sulfur

detected in the SEI film strongly supports the belief that sulfur dioxide molecules have been involved in developing the passivation film. More importantly, Figure 10g clearly visualizes the uniform distribution of elemental sulfur in SEI film, which means the chemical reaction between sulfur dioxide and lithium metals homogeneously occurs on the lithium surface. For more-detailed analysis of the composition, X-ray photoelectron spectroscopy (XPS) depth profiling was performed from the outer surface to a specific depth of the film on the lithium electrode. Figure 11a in the Supporting Information clearly shows the S 2p bonding signals for the electrodes with sulfur dioxide-doped electrolyte after 9 cycles at 1 mA $cm^{-2}$, which is consistent with the EDS mapping results. The overall peak intensities for S 2p, O 1s, C 1s, and F 1s decrease with the depth, except for the Li 1s 52.3 eV peak, which corresponds to elemental lithium in Figure 11.[56] The representative S 2p spectra of lithium surface before and after 300 s of sputtering are shown in Figures 10h and 10i, respectively. On the outermost surface (Figure 10h), major products are identified as $Li_2S_2O_4$ (166.5 eV), $RSO_2R^*$ (167.5 eV), $Li_2SO_3$ (167.0 eV), and $Li_2SO_4$ (169.5 eV), which are mostly containing S−O bonds.[57−59] It was notable that, as being closer to the lithium metal within the SEI layer (Figure 10i), major products have changed from oxygen-containing compounds to oxygen-free materials such as $Li_2S_2$.[46] The detection of two layers with distinct natures in the surface of the electrode implies the sequential process of the surface film formation on the lithium with the sulfur dioxide doping. We presumed that the initial decomposition products from the sulfur dioxide, which are formed immediately after the contact with lithium metal, undergo serial reactions with the excess amount of lithium metal losing its oxygen bonding, because of the strong reducing property.[57,60] Once lithium metal electrodes are passivated with the oxygen-free materials including disulfide, further deposition of film is expected to occur involving compounds containing S−O bonds to form a second layer.

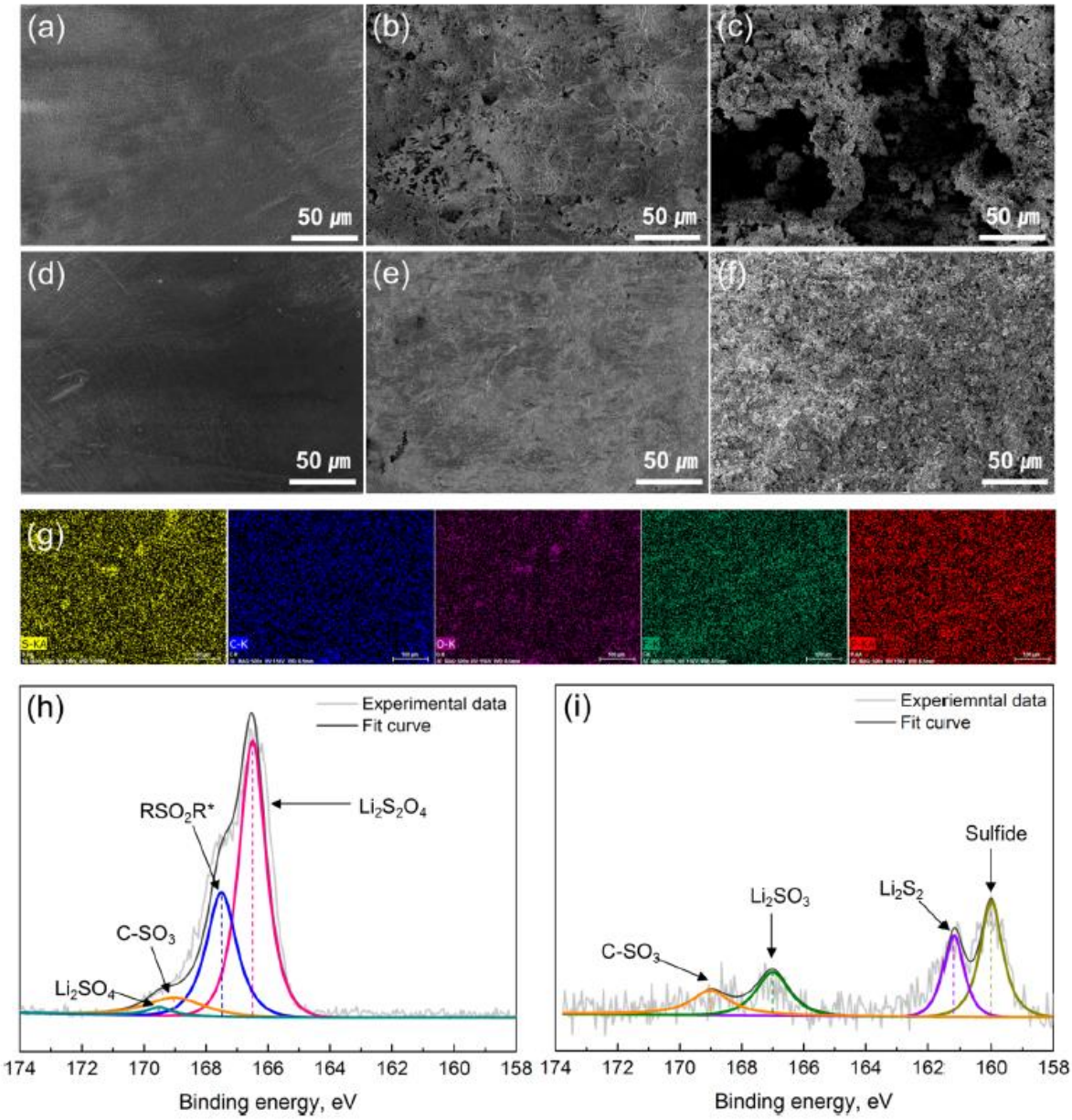


**Figure 10.** SEM images of the surface morphologies of lithium metals (a) before cycle, (b) after 9 cycles, and (c) after 69 cycles in bare cells, as well as (d) before cycle, (e) after 9 cycles, and (f) 69 cycles in sulfur-dioxide-doped cells at a current density of 2 mA $cm^{-2}$. (g) Elemental EDS mapping images of SEI film isolated on stainless steel substrate. Color mapping of yellow, blue, pink, green, and red denote sulfur, carbon, oxygen, fluorine, and phosphorus elements, respectively. The S 2p XPS spectra of the Li electrode (h) before sputtering and (i) after 300 s of sputtering. These XPS specimens, obtained from Li/Li symmetric cells, experienced 9 cycles in sulfur-dioxide-containing electrolytes at 1 mA $cm^{-2}$.

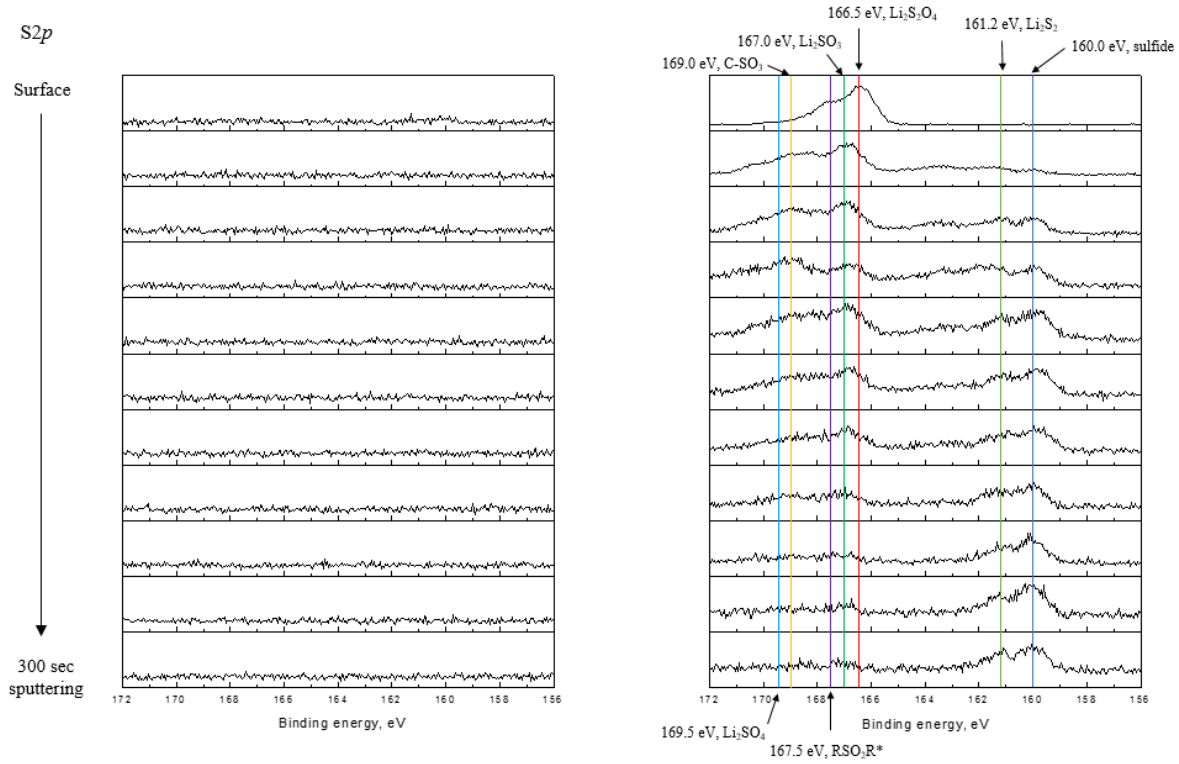


**Figure 11.** (a) XPS Depth profile of S2*p* peak for the lithium surface. (left – bare cell, right – sulfur dioxide doped cell)

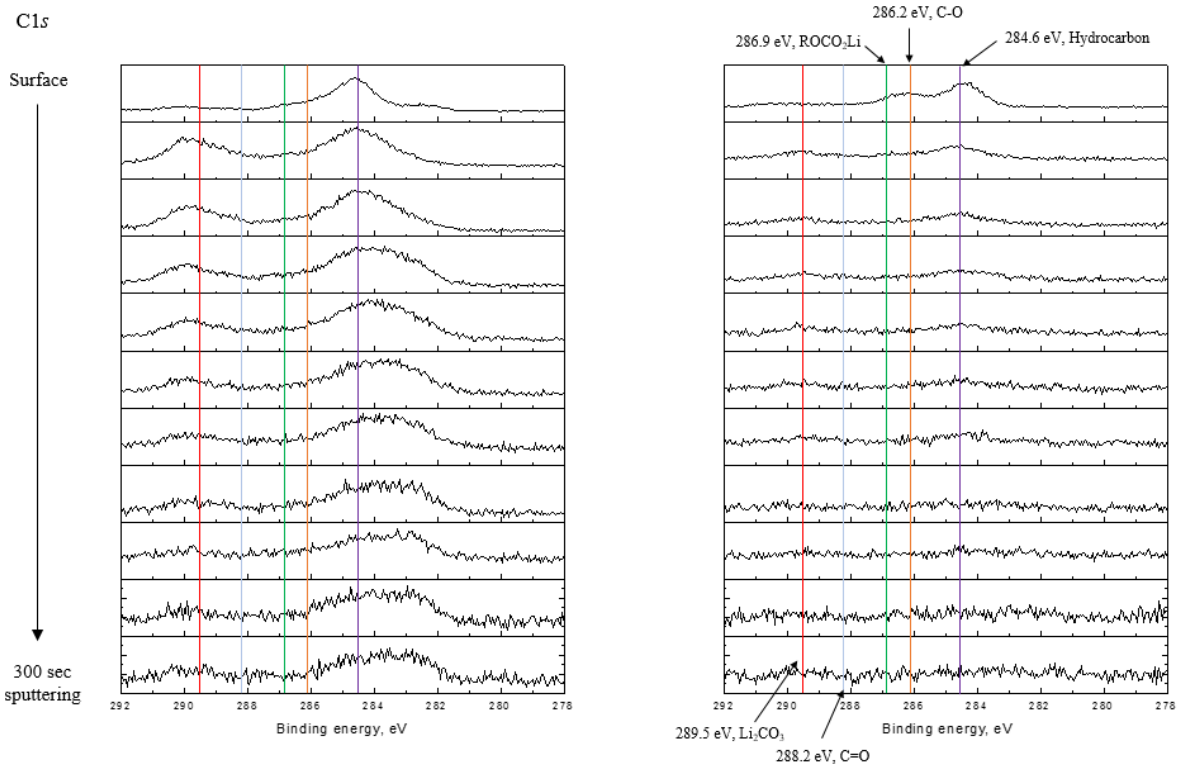


**Figure 11.** (b) XPS Depth profile of C1s peak for the lithium surface. (left – bare cell, right –

sulfur dioxide doped cell)

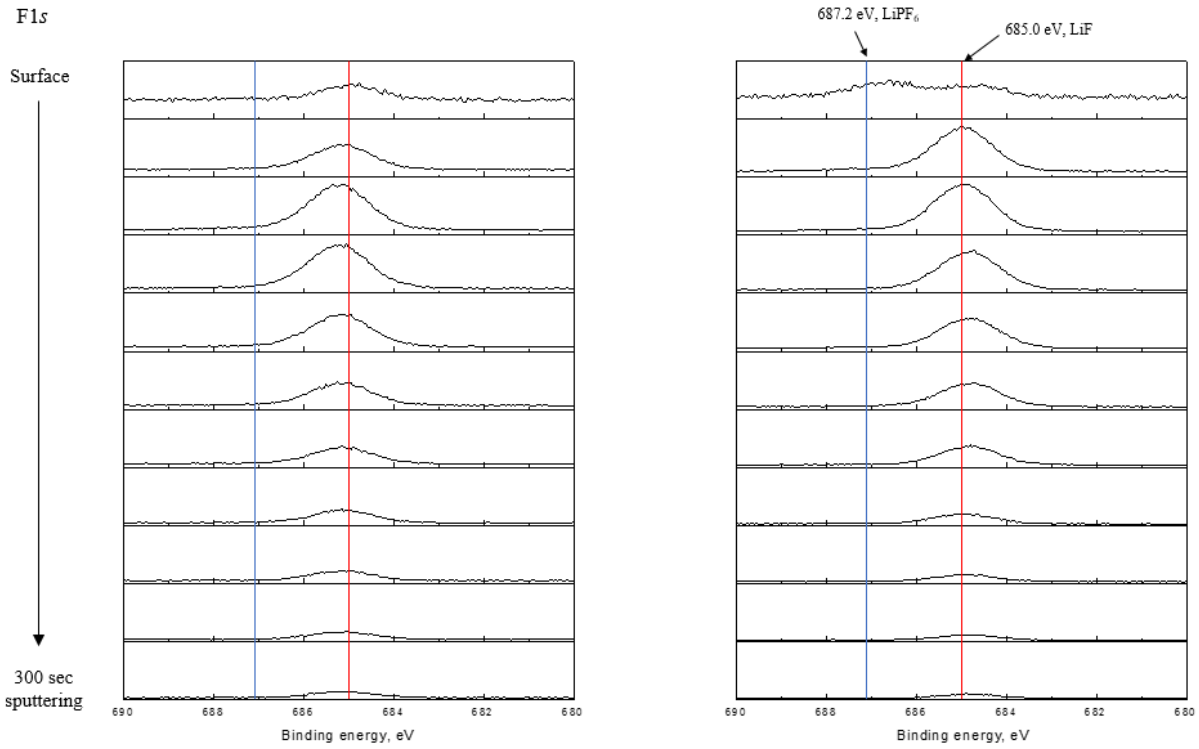


**Figure 11.** (c) XPS Depth profile of F1s peak for the lithium surface (left – bare cell, right – sulfur dioxide doped cell)

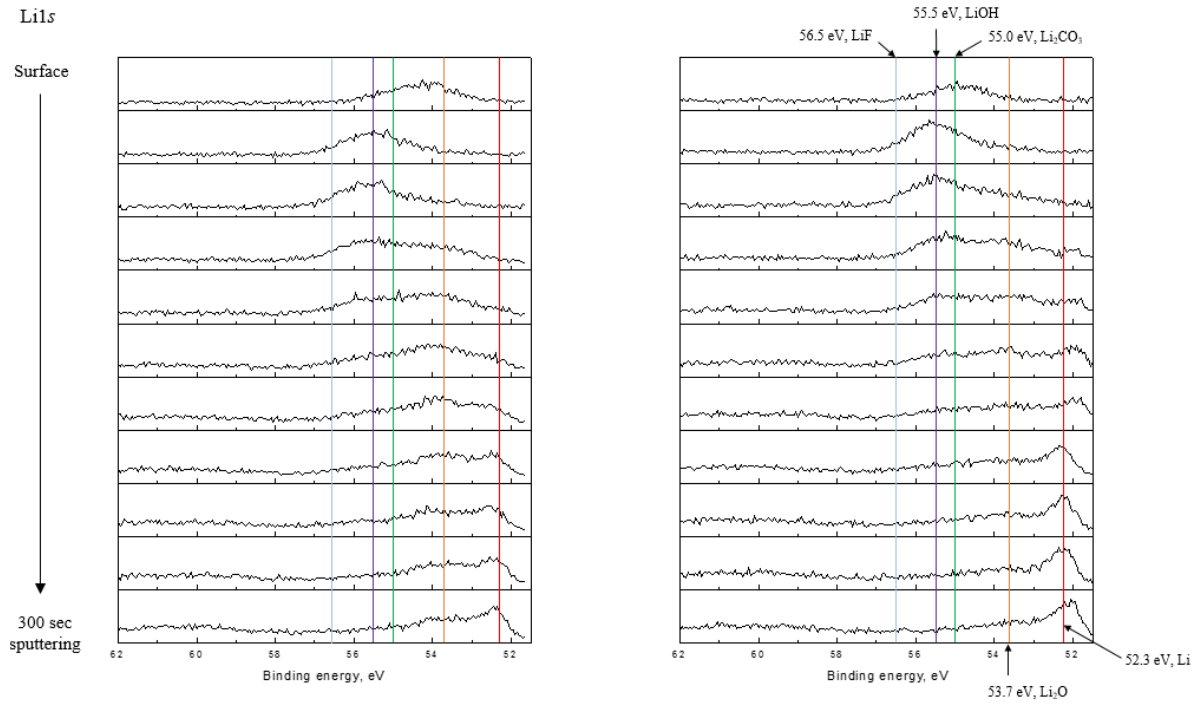

**Figure 11.** (d) XPS Depth profile of Li1s peak for the lithium surface. (left – bare cell, right – sulfur dioxide doped cell)

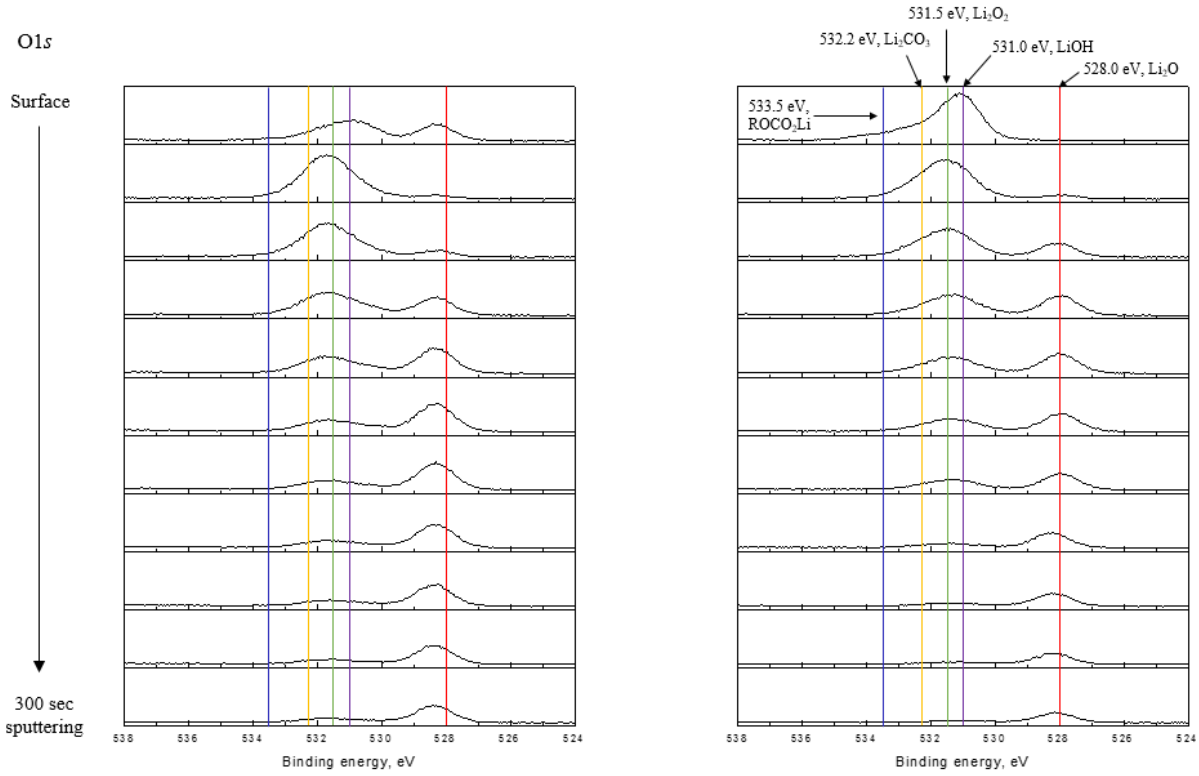


**Figure 11.** (e) XPS Depth profile of O1s peak for the lithium surface. (left – bare cell, right – sulfur dioxide doped cell)

In order to directly probe the efficacy of sulfur dioxide doping in suppressing the growth of the lithium filament, we constructed a simple electrochemical setup as schematically illustrated in the inset of Figure 12a. The symmetric cell contains a donut-shaped ring insulator inserted between two lithium electrodes and the electrical bias was applied to deposit lithium on one of the electrode until it electrically shorts with the counter electrode.[45] The assessment of vertical growth rate, with respect to the planar growth, was possible by measuring the time required for short-circuiting involving sudden voltage drops (see Figures S13a and S13b). Figure 12a presents the short-circuit time ($T_{sc}$) values determined for the electrolytes with and without sulfur dioxide additive at various current densities. Consistent with the Li symmetric cycle results, it was found that the cell with sulfur dioxide doping exhibited much longer $T_{sc}$ values, compared with that of the bare cell, regardless of the applied current densities. Considering the measured Tsc and the distance between

the two electrodes (～200 μm), the vertical growth rate was determined as 0.034 μm/s with sulfur dioxide and 0.476 μm/s without sulfur dioxide, at a same current rate of 1 mA $cm^{-2}$, respectively (see Figure 13c). It confirms that the selective growth was suppressed and the planar growth of lithium metal was comparatively enhanced in the sulfur-dioxide doped cell. Even though the vertical growth rate generally increases with higher current density, sulfur dioxide doping was still effective, even at current rates of 10 mA $cm^{-2}$, exhibiting $T_{sc}$ values that are ～3.6 times higher, compared to the value obtained in bare cells.

### 3.3 Proposed mechanism for the enhanced stability

The premature failure of the electrode in the bare cell is attributed to the uneven surface film randomly formed on the lithium metal, as evidenced from the porous and irregular surface film in Figures 10a−c. The inhomogeneous SEI layer does not allow Li ions to diffuse in and out at identical diffusion rates at the lithium/electrolyte interface, because of the variations in the diffusion length and the conductivity.[61−64] Consequently, Li ions can transport faster where the SEI layer is locally thin and conductive, and preferentially be reduced at the particular lithium surface. Afterward, the selective growth of lithium occurs at the spot where lithium ion flux is locally escalated, as described in Figure 12b.[38,44−46] Moreover, the discriminatory growth is irreversible and rather accelerated due to the bumpy lithium metal morphology that gives rise to self-amplifying lithium deposition by providing a favorable reduction reaction site. On the other hand, the SEI layer formed with the sulfur dioxide additive is believed to be more homogeneous, with respect to the species of constituting compounds and their electrical conductivities, predominantly including analogous sulfur-based compounds such as $Li_2S_2O_4$, $Li_2SO_3$, and $Li_2SO_4$. It is worth mentioning that relatively unusual and conductive sulfur−oxygen compounds are mainly formed with the aid of the sulfur dioxide doping, unlike previous reports exploring the effect of sulfide compounds on lithium metal batteries.[55,65,66] Considering the electrochemically decomposable nature of micrometer-sized $Li_2S_2O_4$ particles as recently reported in lithium−sulfur dioxide secondary batteries, $Li_2S_2O_4$ is regarded to be sufficiently conductive different from well-known insulating SEI components, such as $Li_2CO_3$, LiOH, and $Li_2O$.[67,68] During the initial SEI

construction, the formation of the conductive $Li_2S_2O_4$, the major component of the SEI layer with the doping would promote the development of a uniformly thick SEI layer, because of its capability to efficiently distribute charges. More importantly, the resulting homogeneous SEI layer would be able to transport Li ions at similar diffusion rates to the electrode surface or the electrolyte, thus aiding in the uniform lithium deposition (or stripping) during the electrochemical process (Figure 12c). Even if a new lithium surface is exposed by a momentary nonuniform reaction, residual sulfur dioxide in an electrolyte can additionally react with newly exposed lithium surface to build another uniform interphase during a repeated charge/discharge process. In addition, note that even though lithium sulfur-oxy compounds undergo continuous reactions with lithium metal, as described in Figure 10i, polysulfides such as $Li_2S$ and $Li_2S_2$ that form the inner side of SEI layer are expected to act as beneficial SEI components, as previously reported.[66]

Numerical simulation using a model system shown in Figure 3 supports the beneficial effect of the analogous sulfur-based compounds film on the uniform lithium deposition. (See the Experimental Section for details.) Figures 12d and 12e show snapshots of lithium deposition under different characteristics of SEI layer and compare their behaviors. The existence of irregular SEI layer in Figure 12d (left) promotes the nonuniform growth of lithium deposition, particularly focusing the lithium flux on the locally conductive region, followed by the formation of the protrusion, at the edge of which the lithium growth is also further accelerated. In contrast, lithium grows in a relatively uniform manner if SEI layers are composed of compounds with similar conductivities (Figure 12e). Slight roughening is still observable at the edge of the lithium protrusion described in Figure 12e; however, the effectively larger lithium deposition areas are well maintained without significant local high lithium flux. The initial nonuniformity of SEI layer in its thickness, component and the conductivity naturally leads to the preferential lithium growth and intensifies the nonuniformity of SEI further, which accounts for the irregular shape of lithium, as shown in Figure 12d. The formation of the $Li_2S_2O_4$ and similar sulfur-based compounds layer at the initial surface of lithium metal electrode, in this respect, would be beneficial in mitigating the preferential growth of lithium by providing relatively uniform transport path for Li ions (Figure 12e). We believe that our findings enrich a comprehensive understanding on the precise

role of SEI components on the lithium growth mechanism, with respect to the conductivity property beyond the fact that addition of sulfur dioxide enhances the physicochemical stability of lithium metal.

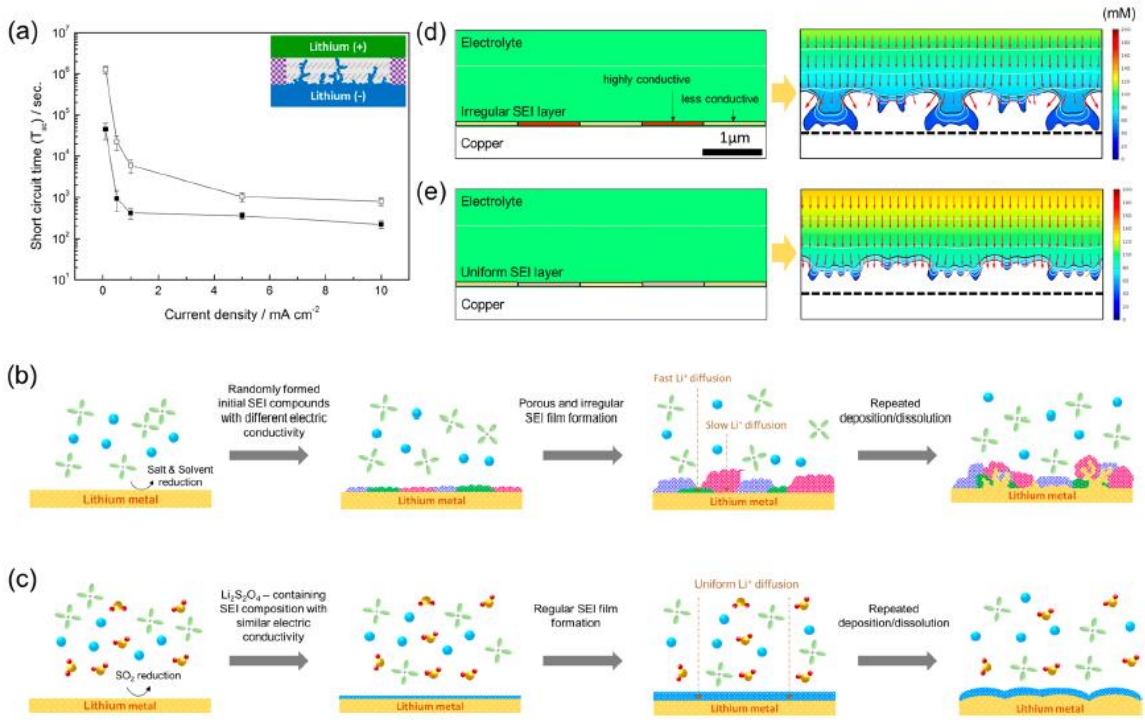


**Figure 4.** (a) Short-circuit time ($T_{sc}$) from galvanostatic measurement for Li/Li symmetric cells with a donut-shaped ring at various current densities ((■) bare cell and (□) sulfur dioxide-doped cell). The cell configuration for the sandwich cell is shown in the inset. Schematic mechanism of repeated deposition/dissolution processes in (b) bare cell and (c) sulfur dioxide-doped cell. Numerical simulation results of Li deposition under (d) irregular SEI and (e) regular SEI layers. Background color indicates the concentration of Li ions. White line is equipotential line in the electrolyte, and the red arrow describes the direction and the size of the current density.

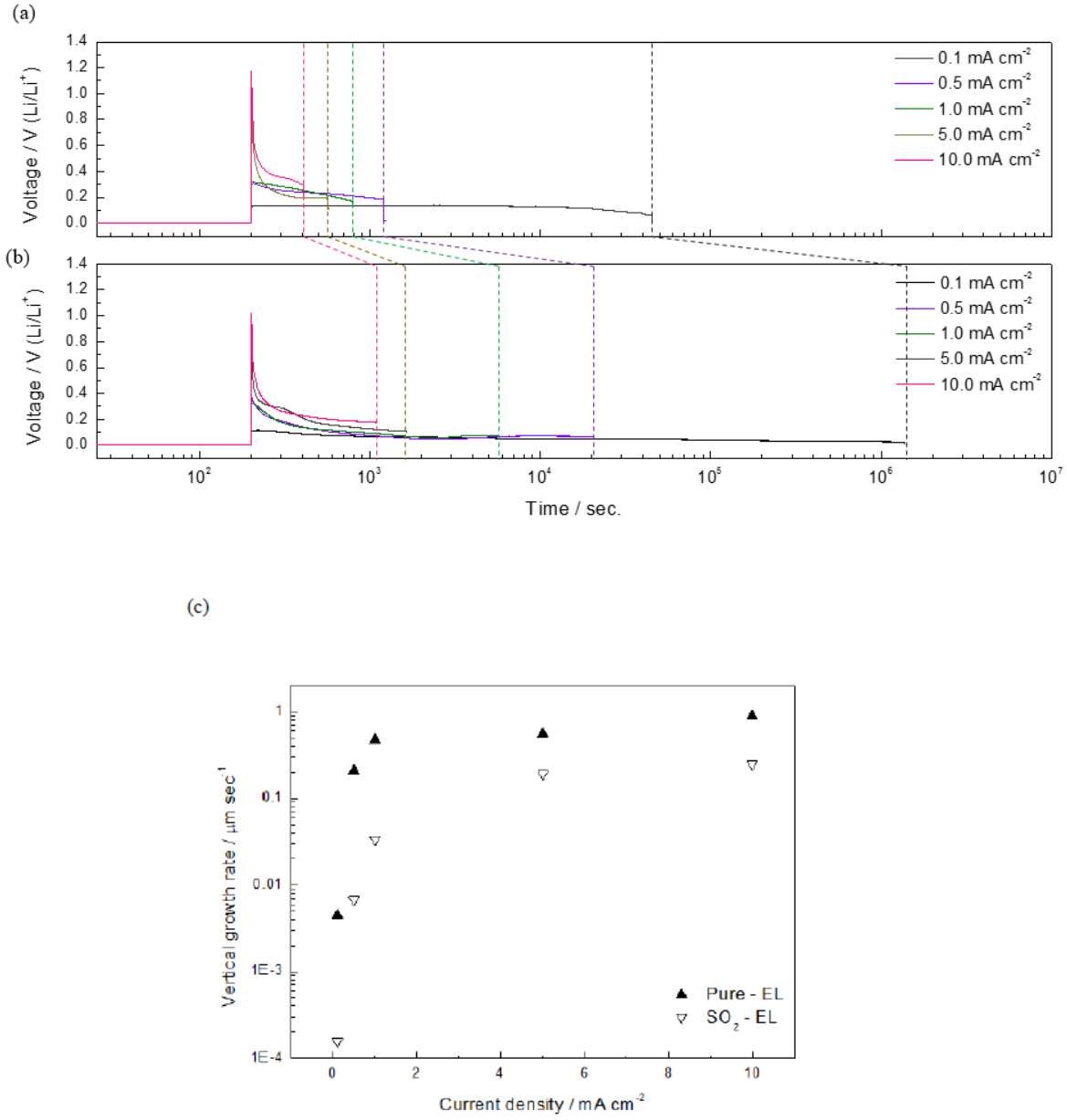


**Figure 13.** Typical time dependent voltage profile of sandwich cells with (a) Bare cells and (b) sulfur dioxide doped cells at different current densities. Dot lines indicate the first voltage fluctuation by internal short circuit. (c) Calculation of vertical lithium growth rate based on $T_{sc}$ values at different current density. (Filled – bare cell, Blank – sulfur dioxide doped cell)

### 3.4 Feasibility of sulfur dioxide additive in practical lithium metal batteries (LMBs)

The feasibility of sulfur dioxide additive in practical lithium metal cell was examined by galvanostatic cycling test of the cell consisting of a $LiCoO_2$ cathode and a lithium metal anode (300 μm thickness) within the voltage window of 3.0−4.2 V. Figure 14a shows the voltage profile

for the initial 2−5 cycles of lithium metal full cell with bare electrolyte and sulfur-dioxide-doped electrolyte. The overall shape of electrochemical profile for both two cells is quite similar; however, it is observed that the sulfur-dioxide doped cell (red curves) delivers a slightly larger capacity, compared to that of cells with undoped electrolyte (blue curves). Moreover, the polarization of the cell with a sulfur dioxide-doped electrolyte is also lower than that of the bare cell during both charge and discharge processes, as shown in Figures 14b and 14c. The voltage curves of the cell containing the sulfur dioxide additive always lie above the blue curves representing the bare cell during every charge process (Figure 14b), whereas the discharge curves of the doped cell are located below those of the cell with bare electrolytes (Figure 14c). This is consistent with the results of impedance measurements showing lower surface resistivity, because of the uniform SEI formation in sulfur-dioxide-doped electrolyte in Figure 6c. The long-term cycle stability of two cells was also provided in Figure 15a. The doped cell exhibits 83.7% of the initial discharge capacity after 350 cycles, which is a notably enhanced capacity retention, compared to 72.6% of the bare cell. Further verification on the viability of sulfur dioxide additive was carried out with LiFePO4 cathode in Figure 15b in the Supporting Information. Analogous to the LMB test with LiCoO2, the LiFePO4 cells with the sulfur dioxide-doped electrolyte also showed an enhanced capacity retention of 93.4% after 350 cycles, whereas the cells with bare electrolyte delivered only 86.5% of the original capacity at the same cycle number. These results support the idea that sulfur dioxide additive could become a universal additive, regardless of the cathode species. Furthermore, EDS measurement confirmed that the sulfur-containing SEI layer is well maintained during the electrochemical cycling and remains intact, even after 350 cycles (see Figure 16).

The galvanostatic life assessment was further investigated in a severe condition of NP ratio 5, as shown in Figure 14d. To achieve such a high NP ratio, 20-μm-thick lithium metal was prepared on copper foil as a negative electrode. Followed by 9 cycles at 1 mA $cm^{-2}$ in Li/Li symmetric cell with the sulfur dioxide-doped electrolyte to make a protection layer, Li metal was reassembled with $LiCoO_2$ cathode, which was evaluated at a 1C-rate. Voltage profiles corresponding each cycle number are provided in Figure 17. Figure 14d shows that the LMB doped with sulfur dioxide

displays a stable cycle life more than 180 cycles, in contrast to the bare LMB. Reversible capacity after 180 cycles of LMBs with and without sulfur dioxide additive was 77.1% and 34.3% of the initial capacity, respectively. The rapid capacity fading and the unstable Coulombic efficiency of the bare LMB originated from the depletion of lithium metal, while $LiCoO_2$ cathode material did not deteriorate noticeably after 180 cycles, which was confirmed in Figure 16a. The unprotected thin lithium metal (20 μm) is likely to consume Li ions in the electrode, as a result of serious side reactions with the electrolyte and the low Coulombic efficiency.

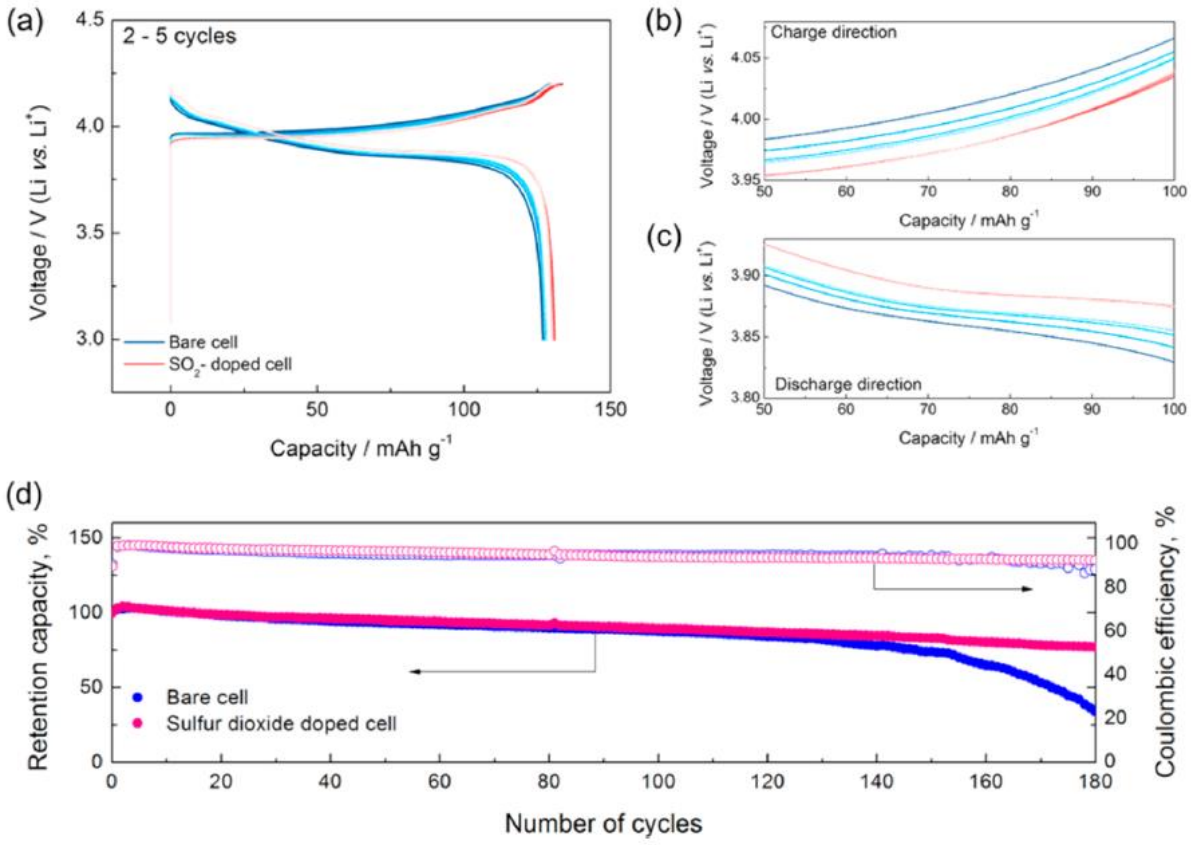

**Figure 14.** (a) Voltage profiles of lithium metal full cells ($LiCoO_2$/300 μm of lithium) for the initial 2−5 cycles. Magnified voltage profiles of (b) charge part and (c) discharge part of panel (a). (d) Retention capacity and Coulombic efficiencies of a $LiCoO_2$/20 μm lithium cell with and without sulfur dioxide doping at 1C-rate (NP ratio 5).

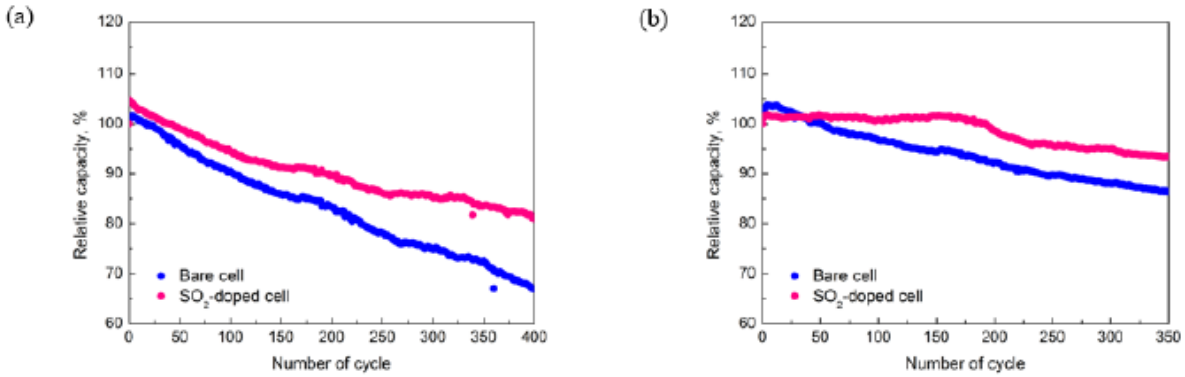


**Figure 15.** Capacity degradation curves of (a) $LiCoO_2$ / lithium metal (300 ㎛) cell (b) $LiFePO_4$ / lithium metal (300 ㎛) cell with a 1 M $LiPF_6$ in EC/DMC (1:1 by volume).

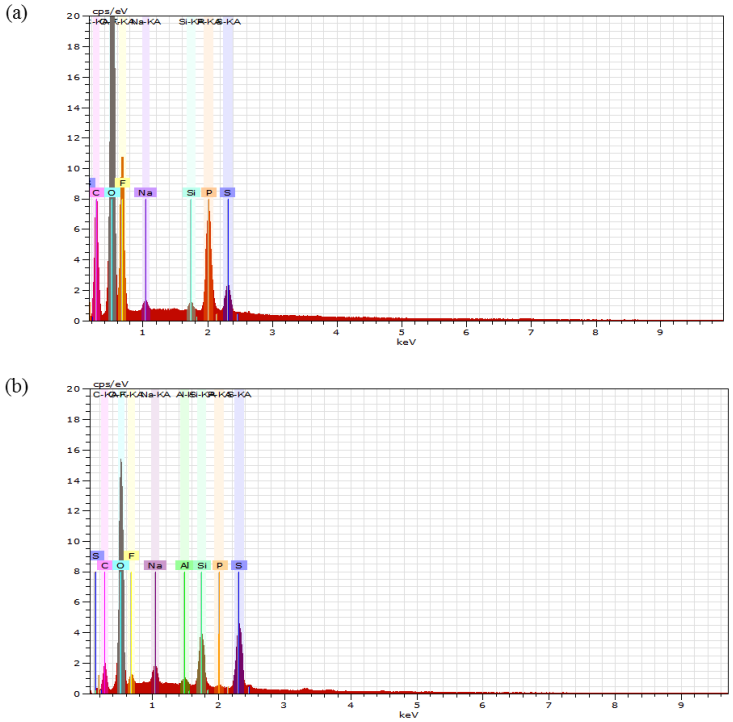


**Figure 16.** Element mapping of lithium surface via Energy-dispersive X-ray spectroscopy (EDS). Each lithium metals were obtained from (a) after 400 cycles of $LiCoO_2$ / Excess lithium metal (b) after 350 cycles of $LiFePO_4$ / Excess lithium metal with a 1 M $LiPF_6$ in EC: DMC (1:1 by volume) with sulfur dioxide modified electrolyte.

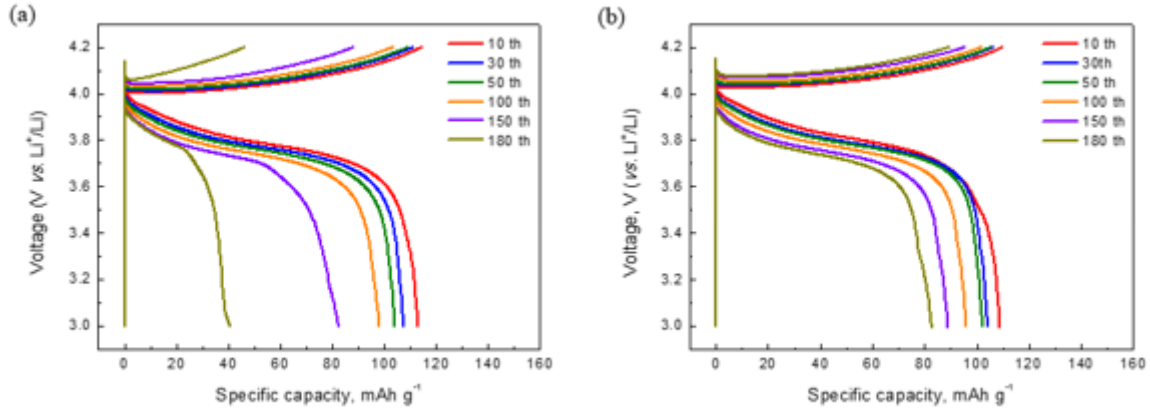


**Figure 17.** Voltage profiles of $LiCoO_2$ / Lithium cell corresponding each cycle numbers (a) without (b) with sulfur dioxide additives under NP ratio 5.

## 4 Conclusion

We successfully employed the gas-phase doping strategy to protect the lithium metal electrode and verified the effectiveness of sulfur dioxide additive in the rechargeable LMB system with noticeable enhancement of cycle life. The combined theoretical and experimental investigation revealed that the formation of analogous sulfur-based compounds film with similar electrical conductivities on lithium metal surface contributed to the development of homogeneous SEI film morphology. This homogeneous SEI film allows Li ions to diffuse at similar rate to the electrode surface or electrolyte, and thus induces the uniform Li deposition reaction during deposition process, as was confirmed by a numerical model calculation. The practical feasibility was verified for LMBs employing conventional cathode materials under severe NP ratio conditions, delivering longer cycle stability and higher Coulombic efficiency for the cell doped with sulfur dioxide additive. Although the presented study using sulfur dioxide additives solely itself might not be a final solution for commercial lithium metal batteries, this facile gas-phase doping can help to develop a more advanced lithium metal battery with synergistic effects, along with other methods, such as supersaturated electrolytes, as preliminarily confirmed in Figure 18 in the Supporting Information. This report is expected to broaden our understanding on the lithium growth mechanism and shed new light on the simple and effective gas-doping strategy to stabilize lithium metal electrodes for lithium batteries.

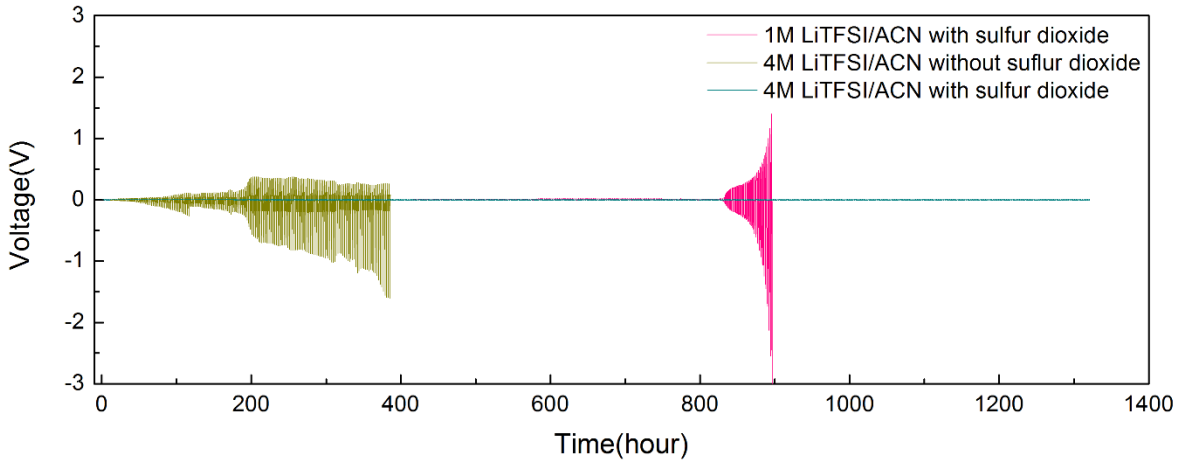


**Figure 18.** Voltage profile of Li-symmetric cell with different electrolyte as a function of operation time. This graph shows the synergetic effect of supersaturated and sulfur dioxide doping.

## 5 References


[1] Xu, W.; Wang, J.; Ding, F.; Chen, X.; Nasybulin, E.; Zhang, Y.; Zhang, J.-G., Lithium metal anodes for rechargeable batteries. Energy Environ. Sci. **2014**, 7 (2), 513-537.

[2] Zhang, K.; Lee, G.-H.; Park, M.; Li, W.; Kang, Y.-M., Recent Developments of the Lithium Metal Anode for Rechargeable Non-Aqueous Batteries. Adv. Energy Mater. **2016**, 6 (20), 1600811.

[3] Armand, M.; Tarascon, J.-M., Building better batteries. Nature **2008**, 451 (7179), 652-657.

[4] Yin, Y. X.; Xin, S.; Guo, Y. G.; Wan, L. J., Lithium–sulfur batteries: electrochemistry, materials, and prospects. Angew. Chem., Int. Ed. **2013**, 52 (50), 13186-13200.

[5] Bruce, P. G.; Freunberger, S. A.; Hardwick, L. J.; Tarascon, J.-M., Li-O2 and Li-S batteries with high energy storage. Nat. Mater. **2012**, 11 (1), 19-29.

[6] Shin, H.-J.; Kwak, W.-J.; Aurbach, D.; Sun, Y.-K., Large-Scale Li-O2 Pouch Type Cells for Practical Evaluation and Applications. Adv. Funct. Mater. **2017**, 27 (11), 1605500.

[7] Liu, Q. C.; Xu, J. J.; Yuan, S.; Chang, Z. W.; Xu, D.; Yin, Y. B.; Li, L.; Zhong, H. X.; Jiang, Y. S.; Yan, J. M., Artificial Protection Film on Lithium Metal Anode toward Long-Cycle-Life Lithium–Oxygen Batteries. Adv. Mater. **2015**, 27 (35), 5241-5247.

[8] Ota, H.; Shima, K.; Ue, M.; Yamaki, J.-i., Effect of vinylene carbonate as additive to electrolyte for lithium metal anode. Electrochim. Acta **2004**, 49 (4), 565-572.

[9] Han, G.-B.; Lee, J.-N.; Lee, D. J.; Lee, H.; Song, J.; Lee, H.; Ryou, M.-H.; Park, J.-K.; Lee, Y. M., Enhanced cycling performance of lithium metal secondary batteries with succinic anhydride as an electrolyte additive. Electrochim. Acta **2014**, 115, 525-530.

[10] Zhang, X.-Q.; Cheng, X.-B.; Chen, X.; Yan, C.; Zhang, Q., Fluoroethylene Carbonate Additives to Render Uniform Li Deposits in Lithium Metal Batteries. Adv. Funct. Mater. **2017**, 27 (10), 1605989.

[11] Naoi, K.; Mori, M.; Naruoka, Y.; Lamanna, W. M.; Atanasoski, R., The Surface Film Formed on a Lithium Metal Electrode in a New Imide Electrolyte, Lithium Bis

(perfluoroethylsulfonylimide)[LiN(C2F5SO2)2]. J. Electrochem. Soc. **1999**, 146 (2), 462-469.

[12] Shiraishi, S.; Kanamura, K.; Takehara, Z. i., Surface Condition Changes in Lithium Metal Deposited in Nonaqueous Electrolyte Containing HF by Dissolution-Deposition Cycles. J. Electrochem. Soc. **1999**, 146 (5), 1633-1639.

[13] Ota, H.; Wang, X.; Yasukawa, E., Characterization of Lithium Electrode in Lithium Imides/Ethylene Carbonate, and Cyclic Ether Electrolytes I. Surface Morphology and Lithium Cycling Efficiency. J. Electrochem. Soc. **2004**, 151 (3), A427-A436.

[14] Kanamura, K.; Tamura, H.; Shiraishi, S.; Takehara, Z.-i., Morphology and chemical compositions of surface films of lithium deposited on a Ni substrate in nonaqueous electrolytes. J. Electroanal. Chem. **1995**, 394 (1), 49-62.

[15] Mogi, R.; Inaba, M.; Jeong, S.-K.; Iriyama, Y.; Abe, T.; Ogumi, Z., Effects of some organic additives on lithium deposition in propylene carbonate. J. Electrochem. Soc. **2002**, 149 (12), A1578-A1583.

[16] Lee, Y. M.; Seo, J. E.; Lee, Y.-G.; Lee, S. H.; Cho, K. Y.; Park, J.-K., Effects of triacetoxyvinylsilane as SEI layer additive on electrochemical performance of lithium metal secondary battery. Electrochem. Solid State Lett. **2007**, 10 (9), A216-A219.

[17] Yoon, S.; Lee, J.; Kim, S.-O.; Sohn, H.-J., Enhanced cyclability and surface characteristics of lithium batteries by Li–Mg co-deposition and addition of HF acid in electrolyte. Electrochim. Acta **2008**, 53 (5), 2501-2506.

[18] Zhamu, A.; Chen, G.; Liu, C.; Neff, D.; Fang, Q.; Yu, Z.; Xiong, W.; Wang, Y.; Wang, X.; Jang, B. Z., Reviving rechargeable lithium metal batteries: enabling next-generation high-energy and high-power cells. Energy Environ. Sci. **2012**, 5 (2), 5701-5707.

[19] Wang, J.; Yamada, Y.; Sodeyama, K.; Chiang, C. H.; Tateyama, Y.; Yamada, A., Superconcentrated electrolytes for a high-voltage lithium-ion battery. Nat. Commun. **2016**, 7, 12032.

[20] Ding, F.; Xu, W.; Graff, G. L.; Zhang, J.; Sushko, M. L.; Chen, X.; Shao, Y.; Engelhard, M. H.; Nie, Z.; Xiao, J., Dendrite-free lithium deposition via self-healing electrostatic shield mechanism. J. Am. Chem. Soc. **2013**, 135 (11), 4450-4456.

[21] Yamada, Y.; Furukawa, K.; Sodeyama, K.; Kikuchi, K.; Yaegashi, M.; Tateyama, Y.; Yamada, A., Unusual stability of acetonitrile-based superconcentrated electrolytes for fast-charging lithium-ion batteries. J. Am. Chem. Soc. **2014**, 136 (13), 5039-46.

[22] Ye, H.; Xin, S.; Yin, Y.-X.; Li, J.-Y.; Guo, Y.-G.; Wan, L.-J., Stable Li Plating/Stripping Electrochemistry Realized by a Hybrid Li Reservoir in Spherical Carbon Granules with 3D Conducting Skeletons. J. Am. Chem. Soc. **2017**, 139 (16), 5916-5922.

[23] Yang, C.-P.; Yin, Y.-X.; Zhang, S.-F.; Li, N.-W.; Guo, Y.-G., Accommodating lithium into 3D current collectors with a submicron skeleton towards long-life lithium metal anodes. Nat. Commun. **2015**, 6, 8058.

[24] Cheng, X.-B.; Hou, T.-Z.; Zhang, R.; Peng, H.-J.; Zhao, C.-Z.; Huang, J.-Q.; Zhang, Q., Dendrite-Free Lithium Deposition Induced by Uniformly Distributed Lithium Ions for Efficient Lithium Metal Batteries. Adv. Mater. **2016**, 28 (15), 2888-2895.

[25] Lee, H.; Lee, D. J.; Kim, Y.-J.; Park, J.-K.; Kim, H.-T., A simple composite protective layer coating that enhances the cycling stability of lithium metal batteries. J. Power Sources **2015**, 284, 103-108.

[26] Zheng, G.; Lee, S. W.; Liang, Z.; Lee, H.-W.; Yan, K.; Yao, H.; Wang, H.; Li, W.; Chu, S.; Cui, Y., Interconnected hollow carbon nanospheres for stable lithium metal anodes. Nat. Nanotechnol. **2014**, 9 (8), 618-623.

[27] Monroe, C.; Newman, J., The impact of elastic deformation on deposition kinetics at lithium/polymer interfaces. J. Electrochem. Soc. **2005**, 152 (2), A396-A404.

[28] Li, Y.; Fedkiw, P. S.; Khan, S. A., Lithium/V6O13 cells using silica nanoparticle-based composite electrolyte. Electrochim. Acta **2002**, 47 (24), 3853-3861.

[29] Kazyak, E.; Wood, K. N.; Dasgupta, N. P., Improved cycle life and stability of lithium metal anodes through ultrathin atomic layer deposition surface treatments. Chem. Mater. **2015**, 27 (18), 6457-6462.

[30] Aurbach, D.; Gamolsky, K.; Markovsky, B.; Gofer, Y.; Schmidt, M.; Heider, U., On the use of vinylene carbonate (VC) as an additive to electrolyte solutions for Li-ion batteries. Electrochim. Acta **2002**, 47 (9), 1423-1439.

[31] Wu, H.-C.; Su, C.-Y.; Shieh, D.-T.; Yang, M.-H.; Wu, N.-L., Enhanced high-temperature cycle life of LiFePO4-based Li-ion batteries by vinylene carbonate as electrolyte additive. Electrochem. Solid State Lett. **2006**, 9 (12), A537-A541.

[32] Ryou, M.-H.; Han, G.-B.; Lee, Y. M.; Lee, J.-N.; Lee, D. J.; Yoon, Y. O.; Park, J.-K., Effect of fluoroethylene carbonate on high temperature capacity retention of LiMn2O4/graphite Li-ion cells. Electrochim. Acta **2010**, 55 (6), 2073-2077.

[33] Liao, L.; Cheng, X.; Ma, Y.; Zuo, P.; Fang, W.; Yin, G.; Gao, Y., Fluoroethylene carbonate as electrolyte additive to improve low temperature performance of LiFePO4 electrode. Electrochim. Acta **2013**, 87, 466-472.

[34] Lee, H.; Choi, S.; Choi, S.; Kim, H.-J.; Choi, Y.; Yoon, S.; Cho, J.-J., SEI layer-forming additives for LiNi0.5Mn1.5O4/graphite 5V Li-ion batteries. Electrochem. Commun. **2007**, 9 (4), 801-806.

[35] Tarnopolskiy, V.; Kalhoff, J.; Nádherná, M.; Bresser, D.; Picard, L.; Fabre, F.; Rey, M.; Passerini, S., Beneficial influence of succinic anhydride as electrolyte additive on the self-discharge of 5 V LiNi0.4Mn1.6O4 cathodes. J. Power Sources **2013**, 236, 39-46.

[36] Qian, J.; Henderson, W. A.; Xu, W.; Bhattacharya, P.; Engelhard, M.; Borodin, O.; Zhang, J.-G., High rate and stable cycling of lithium metal anode. Nat. Commun. **2015**, 6, 6362.

[37] Linden, D.; McDonald, B., The lithium—sulfur dioxide primary battery—its characteristics, performance and applications. J. Power Sources **1980**, 5 (1), 35-55.

[38] Rauh, R.; Brummer, S., The effect of additives on lithium cycling in propylene carbonate. Electrochim. Acta **1977**, 22 (1), 75-83.

[39] Huggins, R., Advanced batteries: materials science aspects. Springer Science & Business Media: **2008**.

[40] Zhang, S. S., Role of LiNO3 in rechargeable lithium/sulfur battery. Electrochim. Acta **2012**, 70, 344-348.

[41] Liang, X.; Wen, Z.; Liu, Y.; Wu, M.; Jin, J.; Zhang, H.; Wu, X., Improved cycling performances of lithium sulfur batteries with LiNO3-modified electrolyte. J. Power Sources **2011**, 196 (22), 9839-9843.

[42] Aurbach, D.; Pollak, E.; Elazari, R.; Salitra, G.; Kelley, C. S.; Affinito, J., On the surface chemical aspects of very high energy density, rechargeable Li–sulfur batteries. J. Electrochem. Soc. **2009**, 156 (8), A694-A702.

[43] Yang, Y.; Zheng, G.; Cui, Y., A membrane-free lithium/polysulfide semi-liquid battery for large-scale energy storage. Energy Environ. Sci. **2013**, 6 (5), 1552-1558.

[44] Song, J.-H.; Yeon, J.-T.; Jang, J.-Y.; Han, J.-G.; Lee, S.-M.; Choi, N.-S., Effect of fluoroethylene carbonate on electrochemical performances of lithium electrodes and lithium-sulfur batteries. J. Electrochem. Soc. **2013**, 160 (6), A873-A881.

[45] Lu, Y.; Tu, Z.; Archer, L. A., Stable lithium electrodeposition in liquid and nanoporous solid electrolytes. Nat. Mater. **2014**, 13 (10), 961-969.

[46] Lim, H. D.; Song, H.; Kim, J.; Gwon, H.; Bae, Y.; Park, K. Y.; Hong, J.; Kim, H.; Kim, T.; Kim, Y. H., Superior rechargeability and efficiency of lithium–oxygen batteries: hierarchical air electrode architecture combined with a soluble catalyst. Angew. Chem., Int. Ed. **2014**, 53 (15), 3926-3931.

[47] Lim, H.-D.; Park, K.-Y.; Gwon, H.; Hong, J.; Kim, H.; Kang, K., The potential for long-term operation of a lithium–oxygen battery using a non-carbonate-based electrolyte. Chem. Commun. **2012**, 48 (67), 8374-8376.

[48] Zaban, A.; Zinigrad, E.; Aurbach, D., Impedance spectroscopy of Li electrodes. 4. A general simple model of the Li-solution interphase in polar aprotic systems. J. Phys. Chem. **1996**, 100 (8), 3089-3101.

[49] Aurbach, D.; Zaban, A., Impedance spectroscopy of lithium electrodes: Part 1. General behavior in propylene carbonate solutions and the correlation to surface chemistry and cycling efficiency. J. Electroanal. Chem. **1993**, 348 (1-2), 155-179.

[50] Aurbach, D.; Zaban, A., Impedance spectroscope of lithium electrodes: Part 2. The behaviour in propylene carbonate solutions—the significance of the data obtained. J. Electroanal. Chem. **1994**, 367 (1-2), 15-25.

[51] Bai, P.; Li, J.; Brushett, F. R.; Bazant, M. Z., Transition of lithium growth mechanisms in liquid electrolytes. Energy Environ. Sci. **2016**, 9 (10), 3221-3229.

[52] Peled, E.; Golodnitsky, D.; Menachem, C.; Bar-Tow, D., An advanced tool for the selection of electrolyte components for rechargeable lithium batteries. J. Electrochem. Soc. **1998**, 145 (10), 3482-3486.

[53] Arora, P.; White, R. E.; Doyle, M., Capacity fade mechanisms and side reactions in lithium-ion batteries. J. Electrochem. Soc. **1998**, 145 (10), 3647-3667.

[54] Thompson, R. S.; Schroeder, D. J.; López, C. M.; Neuhold, S.; Vaughey, J. T., Stabilization of lithium metal anodes using silane-based coatings. Electrochem. Commun. **2011**, 13 (12), 1369-1372.

[55] Li, W.; Yao, H.; Yan, K.; Zheng, G.; Liang, Z.; Chiang, Y.-M.; Cui, Y., The synergetic effect of lithium polysulfide and lithium nitrate to prevent lithium dendrite growth. Nat. Commun. **2015**, 6, 7436.

[56] Kanamura, K.; Shiraishi, S.; Tamura, H.; Takehara, Z. i., X-Ray Photoelectron Spectroscopic Analysis and Scanning Electron Microscopic Observation of the Lithium Surface Immersed in Nonaqueous Solvents. J. Electrochem. Soc. **1994**, 141 (9), 2379-2385.

[57] Abraham, K.; Chaudhri, S., The lithium surface film in the Li/SO2 cell. J. Electrochem. Soc. **1986**, 133 (7), 1307-1311.

[58] Xing, H.; Liao, C.; Yang, Q.; Veith, G. M.; Guo, B.; Sun, X. G.; Ren, Q.; Hu, Y. S.; Dai, S., Ambient lithium–SO2 batteries with ionic liquids as electrolytes. Angew. Chem., Int. Ed. **2014**, 53 (8), 2099-2103.

[59] Agostini, M.; Lee, D.-J.; Scrosati, B.; Sun, Y. K.; Hassoun, J., Characteristics of Li2S8-tetraglyme catholyte in a semi-liquid lithium–sulfur battery. J. Power Sources **2014**, 265, 14-19.

[60] Ein-Eli, Y.; Thomas, S.; Koch, V., The Role of SO2 as an Additive to Organic Li-Ion Battery Electrolytes. J. Electrochem. Soc. **1997**, 144 (4), 1159-1165.

[61] Ryou, M. H.; Lee, D. J.; Lee, J. N.; Lee, Y. M.; Park, J. K.; Choi, J. W., Excellent Cycle Life of Lithium-Metal Anodes in Lithium-Ion Batteries with Mussel-Inspired Polydopamine-Coated Separators. Adv. Energy Mater. **2012**, 2 (6), 645-650.

[62] Elezgaray, J.; Léger, C.; Argoul, F., Linear Stability Analysis of Unsteady Galvanostatic Electrodeposition in the Two-Dimensional Diffusion-Limited Regime. J. Electrochem. Soc. **1998**,

145 (6), 2016-2024.

[63] Léger, C.; Elezgaray, J.; Argoul, F., Dynamical characterization of one-dimensional stationary growth regimes in diffusion-limited electrodeposition processes. Phys. Rev. E **1998**, 58 (6), 7700.

[64] Bard, A. J.; Faulkner, L. R.; Leddy, J.; Zoski, C. G., Electrochemical methods: fundamentals and applications. Wiley New York: **1980**; Vol. 2.

[65] Cheng, X.-B.; Yan, C.; Chen, X.; Guan, C.; Huang, J.-Q.; Peng, H.-J.; Zhang, R.; Yang, S.-T.; Zhang, Q., Implantable solid electrolyte interphase in lithium-metal batteries. Chem **2017**, 2 (2), 258-270.

[66] Cheng, X.-B.; Yan, C.; Peng, H.-J.; Huang, J.-Q.; Yang, S.-T.; Zhang, Q., Sulfurized solid electrolyte interphases with a rapid Li+ diffusion on dendrite-free Li metal anodes. Energy Storage Mater. **2017**, http://dx.doi.org/10.1016/j.ensm.2017.03.008.

[67] Park, H.; Lim, H.-D.; Lim, H.-K.; Seong, W. M.; Moon, S.; Ko, Y.; Lee, B.; Bae, Y.; Kim, H.; Kang, K., High-efficiency and high-power rechargeable lithium–sulfur dioxide batteries exploiting conventional carbonate-based electrolytes. Nat. Commun. **2017**, 8, 14989.

[68] Lim, H. D.; Park, H.; Kim, H.; Kim, J.; Lee, B.; Bae, Y.; Gwon, H.; Kang, K., A New Perspective on Li–SO2 Batteries for Rechargeable Systems. Angew. Chem. **2015**, 127 (33), 9799-9803.

# Abstract in Korean

## 초록

최근 증가된 이차전지에 대한 수요는 지속적으로 높은 에너지 밀도에 대한 연구 개발의 필요성을 높여왔다. 이러한 관점에서 높은 에너지 밀도 (3860 mAh/g)와 가장 낮은 환원전위 (−3.040V *vs.* SHE)를 갖는 리튬 금속은 현재 사용되고 있는 흑연 (372 mAh $g^{-1}$) 기반의 음극물질 보다 10배 높은 에너지밀도를 달성할 수 있기 때문에 이상적인 배터리의 음극 소재로서 각광받고 있다. 하지만, 이러한 장점에도 불구하고 리튬 금속의 높은 반응성과 불균일한 계면반응은 리튬 금속의 연구를 제한 시켜 왔다. Protuburant tip 이라고 불리는 조그마한 불균일성이 발생하게 되면, 전체적인 반응의 균일성은 깨어지고 가속화된 불균일 반응으로 덴드라이트의 성장을 야기시킨다. 점차적으로 성장한 덴드라이트는 양극과 음극을 물리적으로 분리해 놓는 고분자 분리막을 뚫고 성장하여 내부 단락을 통한 배터리의 폭발을 야기하게 된다.

지난 수십년간 리튬 금속을 음극소재로 사용하기 위해 리튬 금속이 가지고 있는 만성적인 문제를 해결하기 위한 다양한 물리적/화학적 방법들이 제안 되어져 왔다. 대표적인 물리적 방법으로서 견고한 고체전해질 계면(SEI) 피막 형성을 위한 유기물/무기물 복합체 코팅과 균일한 반응을 유도하기 위한 3차원 current collector 등이 있다. 다만, 이러한 물리적 방법은 프로세스가 복잡하고, 고비용을 요구하는 특징 때문에 연구가 제한 되어져 왔다. 그래서 상대적으로 낮은 비용으로 접근가능한 첨가제를 이용한 화학적 접근 방법에 대해서는 다양한 개선법이 연구 되어져 왔다. 하지만, 이 또한 리튬 금속의 균일한 반응을 유도할 수는 있으나, 첨가제 등의 부작용으로 인해 이온 전도도 하락 및 전기화학 안전성을 침해 하는 등의 성능 저하를 피할 수는 없었다. 따라서, 리튬 금속을 보호하고 균일한 반응을

유도할 수 있는 새로운 접근법에 대한 연구의 필요성이 지속적으로 대두 되어져 왔다.

본 연구에서는 기존에 연구되어져 왔던 고체 형태의 첨가제 형태를 벗어나, 기체 상태인 아황산가스($SO_2$)를 전해액 내로 첨가하여 리튬 금속 표면을 안정화 시킬 수 있는 방법에 대해서 제안하고자 한다. 아황산가스($SO_2$)는 대부분의 유기 용매에 높은 용해도를 가지기 때문에, 일반 고체 첨가제와 달리 전해액의 점도나 이온전도도의 특성을 유지한채로 높은 함량의 첨가제를 전해액내로 도핑 시킬 수 있게 된다. 이렇게 첨가된 아황산가스($SO_2$)는 리튬 금속과 반응하여 $Li_2S_2O_4$와 같은 전기전도성이 우수한 피막을 형성하게 되어, 아주 균일한 SEI film을 형성하여 리튬 금속의 화학적 안정성을 높여줄 뿐만 아니라 고체전해질 계면층(SEI film) 내의 균일한 리튬 이온의 이동으로 인해 균일한 리튬 금속 반응을 유도할 수 있게 된다. 본 연구에서는 최초로 아황산가스($SO_2$) 가스 첨가제에 대한 영향을 실험적 데이터를 기반으로 메커니즘을 제안하였을 뿐만 아니라, Computational 시뮬레이션을 통해 리튬 이온의 증착 거동을 예측하여 아황산가스($SO_2$)기상 첨가제에 대한 포괄적인 이해를 제공하였다.

**주요어** : 리튬금속 이차전지, 아황산가스, 가스 첨가제, 가스상 도핑, 고체전해질 계면층, 화학적/물리적 안전성, 균일한 리튬 확산

**학번** : 2016-20850